UNIVERSITY OF COPENHAGEN
FACULTY OF SCIENCE

Master's Thesis

Understanding the Gatemon

Investigating why the Gatemon has a lower than predicted coherence time

Markus Nygaard Pedersen

Advisor: Karsten Flensberg

Submitted: May 21, 2024

Abstract

This thesis sets out to explain why experiments with the gatemon qubit have yielded lower than predicted T_1 times. To do this it gives a short introduction to circuit QED and the transmon qubit. Then it presents two different models for the InAs nanowire junction used in gatemons. One model was derived by C.W.J. Beenakker which uses scattering matrix formalism to derive the energies of the bound states. The other one was derived by D.V. Averin and models the nanowire as a quantum point contact that can be Coulomb blocked. Multiple sources of noise are considered, both general types of noise such as $1/f$ and ohmic, and circuit specific sources from components coupled to the qubits. To solve these models numerical methods are presented as the models are not analytically solvable.

In investigating the general types of noise we found that with equal capacitive energy and the same operating frequency Averin's model results in a lower T_1 time. When the transmission is low then the difference in T_1 time is a factor 3 to 4 which is consistent with what experimentalists have found. This indicates that the discrepancy between the current theory and experiments could stem from the fact that the nanowire acts as a quantum point contact and is therefore better described by Averin's model than Beenakker's, which is the one widely use now.

In doing circuit analysis it was found that any loss from adding a drive line to a high frequency qubit can mitigated by increasing the capacitive coupling to ground. There is no evidence that this limits the gatemon, and so it might be a useful insight for other high frequency qubit designs.

Acknowledgments

I would like to thank Karsten Flensberg for firstly introducing me to the fascinating world of superconductivity as a lecturer and later for taking me on as master student so I could help conduct research in the deeply fascinating field superconducting qubits. We have had many great discussions that I have learned immensely from.

Anders Dahl deserves a special thanks for being the one I could always go to for big or small questions both about physics and other stuff like running, and just in general being great company. Anders and Svend Krøjer can claim credit putting me on the path of working with superconducting qubits. Without them this thesis would not have been written.

I would like to thank Benjamin Jocke for being very generous with his time and giving me advice in this thesis which really improved the final product, and in general being an excellent office mate.

Morten Kjaergaard, Zhenhai Sun, David Bofill and Casper Wied have been instrumental in helping me connect the theoretical work in this thesis to what is going on in the laboratory so that this work can be as useful as possible. Especially thank you to David Bofill for letting me use images of his gatemon devices.

I would like to thank my parents for supporting me so that I could dedicate as much time as possible to working on this thesis. Finally to all the people who I have met during the last five years, the great company and good times have helped carry me to the finish line.

Contents

Chapter 1

Introduction

As we are pushing the performance of our computers further and further, and making transistors smaller and smaller, we are approaching the quantum mechanical regime where what we have classically done starts to break down. For many decades the improvements in classical computers has followed Moore's law which states that the amount of transistors on an integrate circuit will double every two years. We are reaching a point where this is no longer possible because the transistors are getting so small that effects such as quantum tunnelling become a real concern. But even though the size of our transistors are reaching a limit, the complexities of our problems are not. As we want to solve more and more complex problems in medicine, cryptography among other fields the performance of current supercomputers cannot keep up. It is simply not feasible to continue designing new computers where the cost of computation goes up exponentially with computation complexity[1].

Quantum computers have the potential to solve these incredibly complex problems for us since performance of quantum computers scale exponentially, not linearly with the addition of extra qubits. An example of such a problem is protein folding. This is hard because of the many ways a protein can fold up on it self and the shape is essential for the proteins function. Even in simplified models this NP hard problem is extremely difficult for classical computers[2]. Protein folding is not the only field within medicine that can benefit from quantum computers. They could help us design better cancer therapy[3]. Since 1997 when Peter W. Shor came up with Shor's algorithm for prime factorisation, the possibility of quantum computers breaking all our current encryption protocols has loomed[4]. But they also offer new types of encryption with quantum encryption protocols such as the BB84 protocol[5].

A quantum computer does not operate with only 1's and 0's. What sets them apart is the possibility of putting a quantum bit (qubit) in a superposition of 1 and 0. So now we have $|1\rangle$ and $|0\rangle$ and any linear combination of them $\alpha|0\rangle + \beta|1\rangle$. This gives us the advantage of being able to use quantum effects such as entanglement and interference. But the unfortunate fact is that these qubits are very delicate and it is easy disturb them and ruin the computation. So we have a fundamental trade-off when designing qubits, which is that for them to be stable they need to be isolated, but if they are completely isolated then we cannot

use them for computation. So to use the qubits properly we need to understand how the surrounding environment affects them so we can isolate them as much as possible and still interact with them when we need to. The problem of keeping a qubit stable, so longer and more complex computations can be completed, can be compared to trying to balance a pencil on your finger in a storm. If we do nothing the pencil will quickly tip over, but if we isolate it by going inside, then it will stay up a bit longer.

There are many prospective platforms for realising quantum computers. Trapped ions, spins, quantum dots and superconducting qubits are all possible candidates for a quantum computer[6]. Superconducting qubits which show great promise are the focus of this thesis. These qubits work by engineering a mesoscopic circuit and then use the mesoscopic wavefunction in superconducters. Manipulating this mesoscopic wavefunction we can get quantum mechanical behaviour in much larger systems than we are used to.

The transmon is one of the most succesful designs for superconducting qubits and is used extensively by for example IBM to build their quantum computers[7]. The disadvantage of transmons is that to be able to tune their frequency we need to introduce a SQUID which is controlled through an external magnetic field. This introduces an extra source of noise from the magnetic fields. Using the pencil analogy again this is like now also standing next to a busy road in addition to the windy weather.

The gatemon is an interesting alternative because it offers the possibility of having a tunable qubit without the need of an external magnetic flux. It is extremely practical to have qubits where you can tune the operating frequency. This means that they can be tuned in and out of resonance with each other.

Gatemons get around this by introducing a semiconductor into the circuit which by controlling the transmission coefficients, gives us control of the frequency such that we avoid external magnetic fields. The transmission can be controlled through a gate voltage which changes the current carrier density. When gatemons have been manufactured and tested it turns out that they have significantly lower T_1 times than predicted. Depending on the device their coherence times are 2 to 5 times lower than what the current theory by Beenakker predicts.

In this thesis we investigate how noise affects the Gatemon qubit and what could be the source of the lower than expected coherence time. Looking at images of gatemon circuits we will construct a circuit model that represents the surrounding environment to see how it affects T_1. We will also be investigating ohmic and $1/f$ noise which in the pencil analogy is understanding which way the wind is likely to blow so we can shield the pencil from it.

Chapter 2

Circiut QED and qubits

2.1 cQED

Circuit quantum electrodynamics (cQED) is the field of physics describing the behaviour of quantum mechanical electrical circuits. cQED springs from cavity QED where one places an atom into a cavity couples to the system through photons[8, 9]. The cavity ensures that the atom is mostly isolated from the environment. In cavity QED this can be an optical cavity which will reflect any photons trying to escape, back to the atom. cQED uses a similar language as the discrete energy spacing in mesoscopic superconducting qubits can be mapped to the energies of an atom. For this reason superconducting qubits are sometimes called artificial atoms. To describe the dynamics of quantum systems we need a Hamiltonian. In this chapter we will derive expressions for the energy of a capacitor, inductor and Josephson junction, and how to combine them to construct the Hamiltonian.

When describing these superconducting circuits we use the lumped element model. In the lumped element model it is assumed that the wavelength of the operating frequency of the circuit is much larger than the circuit. If this was not true and the distance across a capacitor was larger than the operating wavelength of the system, the dynamics become significantly more complicated and we would have to use the full machinery of Maxwell's equations. The lumped element approximation is valid in the circuits that we will look at in this thesis because the circuits we are interested in are operated in the gigahertz range which gives a wavelength on the order of centimetres, which is several orders of magnitude larger than the circuit size which is on the order of micrometers. This means that we will lump all the resistances, inductances and capacitances into ideal components that are then connected by perfect wires that have zero resistance, inductance and capacitance.

To derive the energies we define a variable ϕ that is the generalised coordinate for the circuit,

$$\phi(t) = \int_{-\infty}^{t} V(t')dt', \tag{2.1.1}$$

where $V(t')$ is the voltage over a given component like a capacitor or a resistor. ϕ is called the generalised flux and Equation (2.1.1) gives us the change in it over a given component, like an inductor or a resistor. When applied to an inductor this

is essentially Faraday's law, but here we extend it to all components, that is why it is the generalised flux instead of the magnetic flux. For an ideal linear capacitor the voltage is across it is[10],

$$V(t) = \frac{Q(t)}{C}. \tag{2.1.2}$$

C is the capacitance and $Q(t)$ is the charge on the capacitor which can vary in time. Using Equation (2.1.1) we get the following equation for the generalised flux over a capacitor,

$$\dot{\phi}(t) = V(t) = \frac{Q(t)}{C}. \tag{2.1.3}$$

The boundary term at $-\infty$ vanishes because we assume that at $t = -\infty$ the system was in a state with no voltages and no stored energy. With the charge we can calculate the electrical current, which is the time derivative of charge,

$$I(t) = C\ddot{\phi}(t). \tag{2.1.4}$$

We now have everything we need to describe how much energy is stored in the capacitor as a function of ϕ. The power is given by $P(t) = V(t)I(t)$ and we then integrate it from $-\infty$ to t to find out how much energy is stored in the component. The integral can be solved using integration by parts and using the fact that the boundary term vanishes we arrive at,

$$E_{\text{Cap.}} = \int_{-\infty}^{t} dt' V(t')I(t') = C\int_{-\infty}^{t} dt' \ddot{\phi}\dot{\phi} = \frac{1}{2}C\dot{\phi}^2, \tag{2.1.5}$$

which is the capacitive energy also called the charging energy. A similar calculation can be carried out for an ideal linear inductor with inductance L which has the current-flux relation,

$$I(t) = \frac{1}{L}\phi(t). \tag{2.1.6}$$

Using this and Equation (2.1.1) on the form $\dot{\phi} = V(t)$ the energy stored in the inductor can be found to be,

$$E_{\text{Ind.}} = \int_{-\infty}^{t} dt' V(t')I(t') = \frac{1}{L}\int_{-\infty}^{t} dt' \dot{\phi}\phi = \frac{1}{2L}\phi^2. \tag{2.1.7}$$

The last component that we will use is our circuits is the Josephson junction. To do that we us the two Josephson relations[11],

$$I = I_c \sin(\phi) \quad \text{and} \quad V = \frac{\hbar}{2e}\frac{\mathrm{d}\phi}{\mathrm{d}t} \rightarrow \phi = \frac{2eV}{\hbar}t. \tag{2.1.8}$$

I_c is the critical current of the superconductor, e is the electron charge and $\hbar$ is the reduced Planck's constant. With that we can calculate the energy just as in Equation (2.1.5) and (2.1.7).

$$E_{\text{Jos.}} = \int_{-\infty}^{t} dt' \frac{\mathrm{d}\phi}{\mathrm{d}t'} I_c \frac{\hbar}{2e}\sin(\phi) = -E_J\cos(\phi), \tag{2.1.9}$$

where $E_J = I_c\Phi_0/2\pi = I_c\hbar/2e$ is the Josephson energy and $\Phi_0 = h/2e$ is the superconducting magnetic flux quantum, which has a factor of two as opposed to the normal magnetic flux quantum h/e. This is because in the superconductor all the electrons are coupled in Cooper pairs so the effective charge quantum is $2e$ instead of e.

Now we have expressions for the energy in the components as a function of the change in the generalised fluxes. But when we construct the Lagrangian for a given circuit we have to keep in mind that these fluxes are not completely independent. If we have two components in parallel the flux difference is the same over both because the voltage drop is the same over both. If they are in series then there is one flux difference over the first component and then a second flux difference over the second component and the total flux difference over both components is the sum of the individual flux differences. See for example the LC circuit in Figure 2.1a, the difference in flux is the same over both the capacitor and the inductor. It is very similar to how we work with voltages in classical circuit theory. We will not delve into further details on this subject as further discussion of it is not relevant for the simple circuits that we concern ourselves with in this thesis. Methods on how to analyse more complicated circuits can by found in Aumann et al. and Vool & Devoret[12, 13].

2.2 The transmon and other qubits

2.2.1 LC circuit

One of the simplest circuits we can construct is the LC circuit. The LC circuit as the name implies simply consists of an inductor and a capacitor in an loop as seen in Figure 2.1a. There is just one flux difference which is the difference between the bottom and top parts of the circuit. We then use Equation (2.1.5) and (2.1.7) to write the Lagrangian, where the capacitive energy takes the role of the kinetic energy and the inductive energy takes the role of the potential energy. In the LC circuit it does not matter what we choose, but later when we introduce the Josephson junction it will be the natural choice to let the capacitive energy take the role of kinetic energy.

$$L = \frac{1}{2}C\dot{\phi}^2 - \frac{1}{2L}\phi^2. \tag{2.2.1}$$

We then use a Legendre transformation to find the conjugate variable,

$$\frac{\partial L}{\partial \dot{\phi}} = C\dot{\phi} = Q, \tag{2.2.2}$$

and the Hamiltonian of the system is,

$$H = \dot{\phi}Q - L = \frac{1}{2}C\dot{\phi}^2 + \frac{1}{2L}\phi^2 = \frac{1}{2C}Q^2 + \frac{1}{2L}\phi^2. \tag{2.2.3}$$

This is simply the harmonic oscillator as we would expect from classical circuit theory, and if we promote Q and ϕ to operators we get the quantum harmonic

oscillator. The Hamiltonian for the quantum harmonic oscillator can be rewritten as,

$$H_{\text{H.O.}} = \hbar\omega \left(a^\dagger a + \frac{1}{2} \right), \tag{2.2.4}$$

which has evenly spaced discrete energies $\hbar\omega$ apart. This is a problem though. Because the quantum harmonic oscillator has evenly spaced energies means that it makes a terrible qubit. When designing a qubit we want an isolated two-level system to define our qubit state $|0\rangle$ and $|1\rangle$. One might think that we can simply pick the ground and first excited state and ignore the high energy states, but the even energy spacing makes this impossible. When resonantly driving the quantum harmonic oscillator from the ground state to the first excited state we simultaneously drive higher transitions, for example from the first to the second excited state. One way to avoid this problem would be if the distance from the ground state to the first excited state is not the same as from the first to the second excited state, in short $E_1 - E_0 \neq E_2 - E_1$. If this is the case then the driving pulse that excites the circuit from the ground state to the first excited state will not be able to excite the circuit further because the pulse is off resonance. This helps us to stay in the computational subspace spanned by the two lowest energy states. To break the harmonicity we can switch one of the linear components to a non-linear one. Then the system is no longer a harmonic oscillator and the energy levels will not be evenly spaced any more.

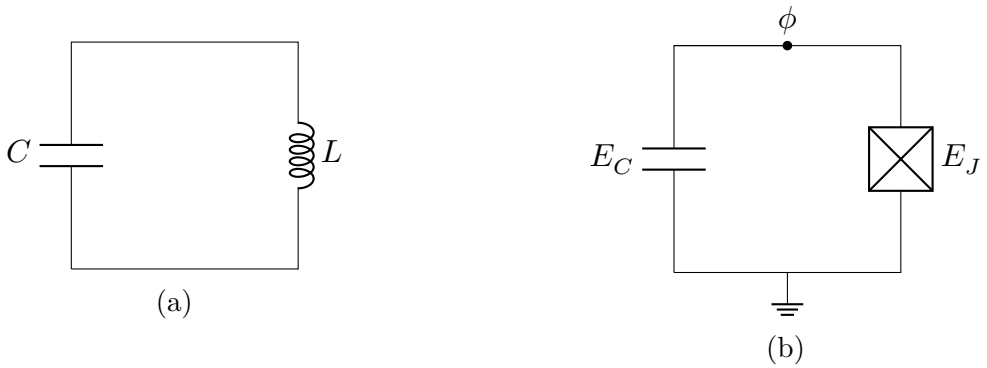

Figure 2.1: **(a)** A LC circuit with capacitance C and inductance L. **(b)** A transmon circuit with the capacitive and Josephson energy marked. The generalised flux is zero at ground and ϕ at the top, so the generalised flux over the components is $\phi - 0 = \phi$.

2.2.2 Transmon

A circuit that is not harmonic can be achieved if we switch out conventional linear inductor (which in normal circuits could be for example a coil) and add in a Josephson junction[14]. A Josephson junction is two superconductors with a thin layer of insulating material between them which allows for the tunnelling of Cooper pairs, but not the flow of conventional current.

We can once again write the Lagrangian and find the Hamiltonian, but since there is no difference in the term that contains $\dot{\phi}$, the calculation is the same as in equation (2.2.3) except switching $\phi^2/2L$ to $-E_J\cos(\phi)$. So the Hamiltonian for the circuit is,

$$\hat{H}_t = 4E_C(n - n_g)^2 - E_J\cos(\phi), \tag{2.2.5}$$

where $E_C = e^2/2C$ is the charging energy of he capacitor, $n = Q/2e$ is number operator for the Cooper pairs, $n_g = C_gV_g/2e$ is the offset voltage in units of $2e$ and ϕ is difference in the generalised flux over the junction.

The off-set charge n_g can come from either a deliberately designed electrode which sets an offset voltage or just from capacitively coupling to the environment around the qubit island. C_g is the capacitive coupling and V_g is the voltage to either ground of the electrode. For example if there is a high voltage around the island, then it can "push" Cooper pairs off the island and change the equilibrium. If E_J/E_C is of the order unity then the circuit is called a Copper pair box. The reason that it is called a Cooper pair box is that as illustrated in Figure 2.1b the bottom part of the circuit is grounded and then the top part acts as an island or box for Cooper pairs where they can only escape if they tunnel through the Josephson junction.

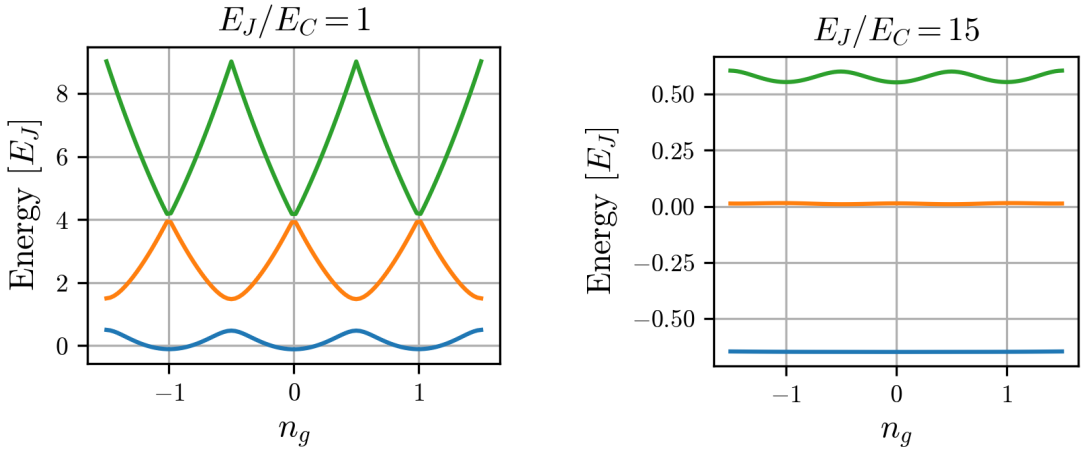

(a) (b)

Figure 2.2: The energies of a transmon at two different values of E_J/E_C. (E_0=blue, E_1=orange and E_2=green).

When $E_J/E_C \gg 1$ the circuit is called a transmon, for most transmons $E_J/E_C \approx 50$. The name transmon comes from the fact that in Koch at al.'s original paper the Cooper pair box is places in a transmission line and that is how they increased the capacitance and therefore increased E_J/E_C [14]. When operated in the transmon regime the transition energies are exponentially insensitive to charge noise. We also loose anharmonicity, but this decrease is only polynomial, so we win more than we loss by increasing E_J/E_C. This decrease in the sensitivity to charge noise can be seen in Figure 2.2 as bands the bands getting flatter as a function of n_g as E_J/E_C increases.

Charge noise i.e. random fluctuations in the charge environment of the qubit, leads to variations in the voltage V_g and in turn (through the capacitive coupling) of the charge offset n_g. Looking at figure 2.2a we see that even small variations in n_g can lead to large variations in the qubit frequency $\omega_q = E_1 - E_0$. This is bad because to use the qubit and perform operations we need to drive it at the right frequency, but if that frequency randomly changes all the time, that becomes very difficult.

A good thing about the $E_J/E_C \approx 1$ regime is that the anharmonicity is very high. Anharmonicity is a measure for how different the transition energies $E_{21} = E_2 - E_1$ and $E_{10} = E_1 - E_0$ are, and is defined as $\alpha = E_{21} - E_{10}$. So for example the harmonic oscillator has $\alpha = 0$ because all the energy levels are evenly spaced and $E_{21} = E_{10}$. On the other hand looking at Figure 2.2a we see that at for example $n_g = 0$ the anharmonicity is very high. The consequence of this is that is when driving the qubit the chance of accidentally driving it further up into E_2 and beyond are virtually non-existent.

Because of their insensitivity to charge noise transmons have enjoyed considerable success and are being used as a major platform for superconducting qubits by big tech companies like Google and IBM[7, 15]. Transmons have many beneficial properties, but the simple transmon in Figure 2.1b has one major shortcoming. It has a fixed frequency set at fabrication. When building quantum computers we want to use many qubits to perform complicated computations. This means that the qubits will need to be coupled together to perform two-qubit gates to entangle them. But we do not want them coupled all the time. Sometimes we need to perform operations on them separately. So we need to be able to turn the coupling on and off. This can be done by turning the coupler on and off, as Google does[15]. In practice it is easier to build a coupler that is on at all times and then tune the qubits. This works because if the qubits are operating at different frequencies they will not "see" each other. We can then tune the frequencies so they match when we need to perform two-qubit gates and tune them away from each other when the operation is done. One way to do this is with flux tunable transmons. These are transmons with two Josephson junctions so they form a SQUID. Changing the external magnetic flux through the SQUID will then change the qubit frequency. The problem with this approach is that it introduces the need to control the magnetic flux through the SQUIDs and this flux will in itself be a new source of noise, flux noise.

Chapter 3

The Gatemon

The Gatemon is almost the same as the transmon. The only difference is that the Josephson junction has been changed. In the transmon there is a conventional Josephson junction, which is two superconductors with a thin layer of insulating material between them which allows for the tunnelling of Cooper pairs. In the Gatemon the insulating layer has been substituted with a semiconductor. This could be an indium arsenide(InAs) nanowire (NW)[16–18]. The thing that fundamentally changes is that when the middle layer is no longer insulating conventional current can to some extent flow. In a semiconductor we can control the transmission by applying a voltage. This is possible because in a semiconductor we can control the carrier density with an electric field. Varying the transmission of the semiconductor will then give us the ability to change the qubit frequency as I will outline below. With this we can now tune the frequencies of our qubits without the need for an external magnetic field, completely eliminating it as a source of noise.

Below I will describe two different approaches to derive the Hamiltonian of the gatemon qubit. One was derived by C.W.J. Beenakker[19] and the other by D.V. Averin[20]. The model that is most often used at the moment is Beenakker's. We will also see if the Averin's model offers a better explanation of the lower than expected coherence times.

3.1 Beenakker

In Beenakker's paper he models the Superconducting-Normal metal-Superconducting (SNS) junction with two perfect Normal metal-Superconducting (NS) boundaries and then a normal scattering region in between as seen in Figure 3.1. Perfect in this context means that at the NS boundary there is no normal scattering and only Andreev reflections are possible. An Andreev reflection happens when an electron is propagating in a normal metal with less energy than the superconducting gap and then hits the NS boundary. In that case the electron does not have enough energy to exist as an electron in the superconductor and immediately couples to another electron and forms a Cooper pair[21]. This bonding to another electron results in a hole being reflected back with the same momentum as the

first electron but in the opposite direction. In between these two NS boundaries he has a region in the normal metal where normal scattering can occur. Normal scattering is like when billiard balls scatter on a billiard table. An electron will come in and hit something and get reflected of into some other direction.

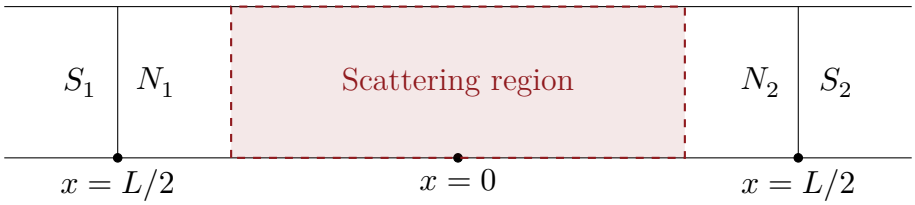

Figure 3.1: Diagram of Beenakker's model with two superconductors S_1 and S_2 with and normal metal in between with either end being the two normal leads N_1 and N_2.

This scattering is caused by the fact that the normal metal is not a perfect crystal, but in reality will have impurities and domain walls. This spacial separation of the two different scattering processes is the key approximation in Beenakker's model. The next step that he takes is then to find the wavefunctions on either side of the boundary. The wavefunctions are two-component wavefunctions because they come from solving the Bogoliubov-de Gennes equation. On the normal side of the boundary there is no potential and no superconducting order parameter Δ so it is just the free particle which in the basis of electrons and holes can be written as,

$$\begin{aligned}\Psi^{\pm}_{\mathrm{n,e}} &= \begin{pmatrix}1\\0\end{pmatrix}\frac{\Phi_n}{k^e_n}\exp\left[\pm ik^{\mathrm{e}}_n(x+L/2)\right],\\ \Psi^{\pm}_{\mathrm{n,h}} &= \begin{pmatrix}0\\1\end{pmatrix}\frac{\Phi_n}{k^h_n}\exp[\pm ik^{\mathrm{h}}_n(x+L/2)],\end{aligned} \tag{3.1.1}$$

in the N_1 lead. $\Phi_n(y,z)$ is the transverse mode, n is the mode index, $k^{\mathrm{e,h}}_n = \sqrt{2m/\hbar^2}\times\sqrt{E_F - E_n + \sigma^{e,h}\varepsilon}$ and $\sigma^e = 1$ and $\sigma^h = -1$. ε is the eigenvalue of the Bogoliubov-de Gennes Hamiltonian, E_n is the threshold energy and E_F is the Fermi energy. The $\pm$ denotes the direction of propagation and for the other normal lead (N_2) Beenakker switches the sign of L. The assumption about the superconducting order parameter $\Delta(x)$ that Beenakker uses is,

$$\Delta(x) = \begin{cases}\Delta_0 e^{-i\phi/2} & \text{for} \quad x < -L/2\\ 0 & \text{for} \quad |x| < L/2\\ \Delta_0 e^{+i\phi/2} & \text{for} \quad x > L/2\end{cases} \tag{3.1.2}$$

One the other side of the boundary in the S_1 superconductor the wavefunction is,

$$\Psi_{n,\mathrm{e}} = \begin{pmatrix}e^{i\eta^e/2}\\ e^{-i\eta^e/2}\end{pmatrix}\frac{1}{\sqrt{2q^{\mathrm{e}}_n}}\frac{1}{(\varepsilon^2/\Delta_0^2-1)^{1/4}}\frac{\Phi_n}{k^e_n}\exp\left[\pm iq^e_n(x+L/2)\right] \tag{3.1.3}$$

with $q_n^{\mathrm{n,h}} = \sqrt{2m/\hbar^2}\sqrt{E_F - E_n + \sigma^{\mathrm{n,e}}\sqrt{\varepsilon^2 - \Delta_0^2}}$ and $\eta^{\mathrm{e,h}} = \phi/2 + \sigma^{\mathrm{e,h}} \arccos(\varepsilon/\Delta_0)$. For S_2 he switches $\phi \to -\phi$ and $L \to -L$. The wavefunction in the superconductor is a superposition of an electron and a hole.

A particle entering the normal region can be a right moving electron or hole in the left lead (N_1) or a left moving electron or hole in the right lead (N_2). So any incoming wavefunction can be described as a superposition of these possibilities and therefore a complete incoming wavefunction can be described by four coefficients $c_{\mathrm{in}} = [c_e^+(N_1), c_e^-(N_2), c_h^-(N_1), c_h^+(N_2)]^T$. After the scattering the wavefunction will then in general end up as a superposition of outgoing wavefunctions described by $c_{\mathrm{out}} = [c_e^-(N_1), c_e^+(N_2), c_h^+(N_1), c_h^-(N_2)]^T$. These two states are then coupled via a scattering matrix which has the constraint that normal scattering does not couple electrons and holes, think back to the example with the billiard balls. When a billiard ball hits the edge of the board a new hole does not suddenly appear. So for example an electron coming from the left lead (N_1) and moving right can either be reflected back and become a left moving electron in the left lead (N_1), or it can pass through the scattering region and become a right moving electron in the right lead(N_2), but it cannot become a hole. This means that the scattering matrix in the normal region is block diagonal and can be written as,

$$S_N(\varepsilon) = \begin{pmatrix} s_0(\varepsilon) & 0 \\ 0 & s_0^*(-\varepsilon) \end{pmatrix} \quad \text{where} \quad s_0 = \begin{pmatrix} r_{11} & t_{12} \\ t_{21} & r_{22} \end{pmatrix}, \tag{3.1.4}$$

where r_{11}, t_{12}, t_{21} and r_{22} all depend in ε. r is the reflection amplitude. It tells us how likely a particle is to be reflected back the way it came from and t is the transmission amplitude and tells us how likely a particle is to pass through the scattering region. So this matrix connects the two states in such a way that $c_{\mathrm{out}} = S_N c_{\mathrm{in}}$. Now the wavefunction as been scattered of some impurity in the normal region and is propagating out towards the NS boundaries. If $\varepsilon > \Delta$ it will simply pass through into the superconductor, if $\varepsilon < \Delta$ then particle does not have enough energy to exist one its own in the superconductor. Since the electron does not have enough energy then it will be Andreev reflected. Andreev reflections couple electrons to holes and visa versa. The boundary is assumed perfect there is no normal scattering and the scattering matrix becomes,

$$S_A = \alpha(\varepsilon)\begin{pmatrix} 0 & r_A \\ r_A^* & 0 \end{pmatrix} \quad \text{where} \quad r_A = \begin{pmatrix} e^{i\phi/2}\mathbb{1} & 0 \\ 0 & e^{-i\phi/2}\mathbb{1} \end{pmatrix}, \tag{3.1.5}$$

for $\varepsilon < \Delta$. This matrix operates on a superposition of outgoing states, so c_{out}, and the states get reflected back towards the normal region which is described by c_{in}. This means that it connects the outgoing to the incoming states such that $c_{\mathrm{in}} = S_A c_{\mathrm{out}}$.

Beenakker then combines $c_{\mathrm{out}} = S_N c_{\mathrm{in}}$ and $c_{\mathrm{in}} = S_A c_{\mathrm{out}}$ to find that a bound state must satisfy $c_{\mathrm{bound}} = S_A S_N c_{\mathrm{bound}}$. This is true because a bound state by definition transitions through a closed loop of states and then must return to the same state again at some point. $c_{\mathrm{bound}} = S_A S_N c_{\mathrm{bound}}$ is the eigenvalue problem with eigenvalue 1 and thus implies $\det(\mathbb{1} - S_A S_N) = 0$. The expression can be generalised to N channels by expanding r_{11}, t_{12}, t_{21} and r_{22} to $N \times$

N matrices. Now he has a partitioned matrix and there exists an identity for partitioned matrices that simplifies the determinant[22].

$$\text{Given} \quad Z = \begin{pmatrix} A & B \\ C & D \end{pmatrix} \quad \text{then} \quad \det(Z) = \det(AD - ACA^{-1}B). \tag{3.1.6}$$

Using this relation he rewrites the determinant

$$\det(\mathbb{1} - S_A S_N) = \det(\mathbb{1} - \alpha^2 r_A^* s_0(\varepsilon) r_A s_0(-\varepsilon)^*) = 0. \tag{3.1.7}$$

Beenakker then makes the approximation that the normal scattering does not change significantly with in the gap so $s_0(\varepsilon) = s_0(-\varepsilon)^* = s_0(0)$ to get,

$$\det\left(1 - \frac{\varepsilon^2}{\Delta^2} - t_{12}t_{12}^\dagger \sin\left(\frac{\phi}{2}\right)^2\right) = 0. \tag{3.1.8}$$

When there is only one channel then this is a 1×1 matrix and solving for ε,

$$\varepsilon = \Delta\sqrt{1 - T\sin(\phi/2)^2}. \tag{3.1.9}$$

where $T = t_{12}t_{12}^\dagger$. If there are several channels the coefficients t_{12} and $t_{12}^\dagger$ becomes matrices themselves. This can be solved in terms of the eigenvalues T_i of the $t_{12}t_{12}^\dagger$ matrix and the bound state energy becomes,

$$\varepsilon = \sum_i \Delta\sqrt{1 - T_i\sin(\phi/2)^2}. \tag{3.1.10}$$

This is the major result from Beenakker's paper, the energy of a Andreev bound state in a SNS junctions. We can then add the capacitive energy between the two superconductors to get the full Hamiltonian of the gatemon qubit,

$$H_B = 4E_C(n - n_g)^2 - \Delta\sum_i \sqrt{1 - T_i\sin(\phi/2)^2}. \tag{3.1.11}$$

This is the Hamiltonian that the experimentalists currently use. It is this equation that predicts the higher T_1 times than are currently observed.

3.2 Averin

Another way of looking at the system is that the nanowire acts as a quantum point contact because it is a constriction between the ground plate and the Cooper pair island. The nanowires are less than the 200nm wide[18] and the effects of quantum point contacts have been observed in constrictions as wide as 360nm[23]. Because the nanowire is a semiconductor we can Coulomb blockade it, which is the system that Averin solved.

We still have a superconductor on either side and they will generally have different superconducting phases. In Averin's model he uses a step-like superconducting phase[20]. Since its is only the difference in phase on either side that has a physical effect the superconducting order parameter can be written as,

$$\Delta(x) = \begin{cases} \Delta & \text{for} \quad x < 0 \\ \Delta e^{i\phi} & \text{for} \quad x > 0 \end{cases}. \tag{3.2.1}$$

He then solves the Bogoliubov-de Gennes equations for both left and right moving particle with this pair potential and finds that the Hamiltonian is,

$$H = 4E_C \left(n - n_g\right)^2 + \sum \varepsilon(\phi) + V, \tag{3.2.2}$$

where $4E_C \left(n - n_g\right)^2$ like in the transmon Hamiltonian is the capacitive energy between the superconductors. Solving the Bogoliubov-de Gennes equations he finds that there exists two sub gap states $\varepsilon^{\pm}(\phi) = \mp\Delta\cos(\phi/2)$. V is the back scattering which depends on the shape of the potential $U(x)$ cross the contact. With this he finds that the only terms of importance in the back scattering are

$$\langle\Psi^-|V|\Psi^+\rangle = ir\Delta\sin(\phi/2), \tag{3.2.3}$$

where $r = -iU(2k_F)/\hbar v_F$ and $|\Psi^{\pm}\rangle$ are the sub gap states with energy $\pm\Delta\cos(\phi/2)$. $U(2k_F)$ is the Fourier transform of the potential $U(x)$. Now the Hamiltonian in ϕ space is,

$$H_A = 4E_C(n - n_g)^2 \otimes I_2 + \Delta \begin{pmatrix} \cos(\phi/2) & -ir\sin(\phi/2) \\ ir\sin(\phi/2) & -\cos(\phi/2) \end{pmatrix}, \tag{3.2.4}$$

where I_2 is the 2×2 identity matrix.

We originally wanted to try and extend Averin's Hamiltonian to more channels with different transmission coefficients just like Beenakker did. We thought that we could take the Kronecker sum by assuming that there was no scattering between channels and therefore they would be independent. Taking the Kronecker sum for two channels would be $H_{tot} = H_{T_1} \otimes I_2 + I_2 \otimes H_{T_2}$ or $H_{tot} = H_{T_1} + H_{T_2}$. The problem with this is the both H_{T_1} and H_{T_2} depend on the same phase difference ϕ. This means that they are not as independent as we first thought and solving this non-trivial problem to combine the Hamiltonians was beyond the scope of this thesis.

Chapter 4

Analytical Calculations

4.1 Comparison in the limits

To get a better understanding of the Hamiltonians it is illustrative to look at the behaviour in the limits. We will look at the heavy limit as it is in this regime that the gatemon is operated. To get a sense of the behaviour when we vary the transmission T of the junction, we will investigate the limits of high and low T. The behaviour in all these limits will be used to verify the validity of the numerical solutions.

4.1.1 The heavy limit

When speaking of the "weight" or "how heavy" a system is we are drawing on the analogy of a mechanical system. Taking the capacitive term (the term containing E_C) to be the kinetic energy, then $E_C = 1/m$. So a heavy system is one where E_C is small. We take Averin's Hamiltonian (3.2.4) in the limit $E_C \ll \Delta$. In this limit we can temporally ignore the kinetic term because it is small compared to the potential and find the eigenvalues of the potential.

$$\begin{aligned} 0 &= \det \begin{vmatrix} \cos(\phi/2) - \lambda & -ir\sin(\phi/2) \\ ir\sin(\phi/2) & -\cos(\phi/2) - \lambda \end{vmatrix} \\ 0 &= -\cos(\phi/2)^2 + \lambda^2 - r^2\sin(\phi/2) \\ \lambda &= \pm\sqrt{1 - T\sin(\phi/2)^2}, \end{aligned} \tag{4.1.1}$$

with $r = \sqrt{1-T}$. So when $E_C \ll \Delta$ we recover Beenakker's potential from Averin's potential if we remove the kinetic term, diagonalise and then reintroduce the kinetic term on the diagonal afterwards. This approach relies on the assumption that any of diagonal terms that would appear from doing the transformation on the kinetic term are very small, which they are for $\Delta \gg E_C$. We will derive these off diagonal terms in Section 4.2.

4.1.2 T limits

We can also look at the limits of T. In the small T limit where the normal metal becomes almost insulating. We Taylor expand Beenakker's Hamiltonian around $T = 0$ to find,

$$\Delta\sqrt{1 - T\sin(\phi/2)^2} = \Delta\left(1 - \frac{T\sin(\phi/2)^2}{2}\right) + \mathcal{O}(T^2) \tag{4.1.2}$$

$$= \Delta\left(1 - \frac{T\frac{1-\cos(\phi)}{2}}{2}\right) + \mathcal{O}(T^2) \tag{4.1.3}$$

$$= \frac{\Delta T}{4}\cos(\phi) + \Delta\left(1 - \frac{T}{4}\right) + \mathcal{O}(T^2). \tag{4.1.4}$$

Doing that we see in the small transmission limit that Beenakker's Hamiltonian resembles the transmon Hamiltonian, except for a constant term that has no impact on the dynamics of the system. This result is exactly what we would expect since when we have a junction with arbitrary transmission and if we let that transmission go to zero, then the junction effectively becomes insulating because no conventional current can flow and only Cooper pairs can tunnel through. But this is just a conventional Josephson junction, so when the transmission T goes to zero we recover the transmon Hamiltonian.

We can also take the opposite limit and set $T = 1$ so that current can flow freely. In that case Beenakker's potential becomes,

$$\Delta\sqrt{1 - T\sin(\phi/2)^2} \to \pm\Delta\cos(\phi/2), \tag{4.1.5}$$

and setting $T = 1$ for Averin's Hamiltonian,

$$\Delta\begin{pmatrix} \cos(\phi/2) & -ir\sin(\phi/2) \\ ir\sin(\phi/2) & -\cos(\phi/2) \end{pmatrix} \to \Delta\begin{pmatrix} \cos(\phi/2) & 0 \\ 0 & -\cos(\phi/2) \end{pmatrix}. \tag{4.1.6}$$

Here the two quasiparticles in Averin's Hamiltonian completely decouple and we get two separate systems. These two system correspond to the solutions of Beenakker's Hamiltonian, so the models are equal, just in slightly different representations. This makes physical sense because if $T = 1$ the scattering normal region in Beenakker's model does not affect the particles and it is only the Andreev reflections that play a part. But the Andreev reflection only depends on ϕ. Likewise, in Averin's model $r = -iU(2k_F)/\hbar v_F$ so if $r = 0$ then $U(2k_F)$ must be zero. The potential plays no role and the only thing left to affect the quasiparticles is the phase difference ϕ.

4.2 Unitary transformation

We will now derive the extra terms that appear from transforming the kinetic term that we ignored in Section 4.1.1. We know from Equation (4.1.1) that we can diagonalise the the potential part of Averin's Hamiltonian to get Beenakker's

potential. This means that there exists a unitary transformation U that solve the following equation,

$$U\begin{pmatrix}\cos(\phi/2) & -ir\sin(\phi/2)\\ ir\sin(\phi/2) & -\cos(\phi/2)\end{pmatrix}U^\dagger = \begin{pmatrix}\sqrt{1-T\sin(\phi/2)^2} & 0\\ 0 & -\sqrt{1-T\sin(\phi/2)^2}\end{pmatrix}. \tag{4.2.1}$$

The unitary transformation that accomplishes this is constructed from the orthonormal eigenvectors,

$$\mathbf{v}_+ = \begin{pmatrix}f_1(\phi)\\ f_2(\phi)\end{pmatrix} \quad \text{and} \quad \mathbf{v}_- = \begin{pmatrix}-f_2(\phi)\\ f_1(\phi)\end{pmatrix}, \tag{4.2.2}$$

where $f_1(\phi)^2 + f_2(\phi)^2 = 1$ for all ϕ. To satisfy this constraint we introduce a new variable $y(\phi)$ and let $f_1(\phi) = \cos(y)$ and $f_2(\phi) = \sin(y)$ so that the eigenvectors become,

$$\mathbf{v}_+ \to \begin{pmatrix}\cos(y)\\ \sin(y)\end{pmatrix}, \quad \mathbf{v}_- \to \begin{pmatrix}-\sin(y)\\ \cos(y)\end{pmatrix}. \tag{4.2.3}$$

Which satisfy the above requirements for any function $y(\phi)$ and therefore

$$U = \begin{pmatrix}\cos(y) & -\sin(y)\\ \sin(y) & \cos(y)\end{pmatrix} = e^{i\sigma_2 y} \tag{4.2.4}$$

where σ_2 is the second Pauli matrix. We will drop the (ϕ) on $y(\phi)$ in equations to make them less cluttered but y still has a ϕ dependency. So there exists a function $y(\phi)$ such that Equation (4.2.1) is true. To find it we can use the fact that U by construction obeys the following equation,

$$UAU^\dagger = E_B\sigma_3. \tag{4.2.5}$$

Where A is the potential in Averin's Hamiltonian (3.2.4) and E_B is the potential in Beenakker's Hamiltonian (3.1.11). Rewriting this equation we get,

$$\begin{pmatrix}\cos\left(\frac{\phi}{2}\right) & r\sin\left(\frac{\phi}{2}\right)\\ r\sin\left(\frac{\phi}{2}\right) & -\cos\left(\frac{\phi}{2}\right)\end{pmatrix} = A = E_BU^\dagger\sigma_3U = \sqrt{1-T\sin\left(\frac{\phi}{2}\right)^2}\begin{pmatrix}\cos(2y) & \sin(2y)\\ \sin(2y) & -\cos(2y)\end{pmatrix} \tag{4.2.6}$$

Matching elements in the matrix we can find and solve for $y(\phi)$,

$$y(\phi) = \frac{1}{2}\arccos\left(\frac{\cos(\phi/2)}{\sqrt{1-T\sin(\phi/2)^2}}\right), \tag{4.2.7}$$

With Equation (4.2.4) and (4.2.7) we can now do the transformation. One thing to keep in mind when we work with operators, is to remember to carry them through. We will use the notation that if the derivative is "empty" on top, then it operates on everything to the right whereas if it is "occupied" then it only operates on what is on the fraction line. For example,

$$\frac{\partial}{\partial\phi}ABC \text{ operates on everything,} \quad \frac{\partial A}{\partial\phi}BC \text{ only operates on } A.$$

Keeping this in mind we can transform the kinetic term,

$$H = U\frac{\partial^2}{\partial\phi^2}U^\dagger \tag{4.2.8}$$

$$= U\frac{\partial}{\partial\phi}\left(\frac{\partial U^\dagger}{\partial\phi} + U^\dagger\frac{\partial}{\partial\phi}\right) \tag{4.2.9}$$

$$= U\frac{\partial^2 U^\dagger}{\partial\phi^2} + U\frac{\partial U^\dagger}{\partial\phi}\frac{\partial}{\partial\phi} + U\frac{\partial U^\dagger}{\partial\phi}\frac{\partial}{\partial\phi} + UU^\dagger\frac{\partial^2}{\partial\phi^2} \tag{4.2.10}$$

$$= \frac{\partial^2}{\partial\phi^2} + U\frac{\partial^2 U^\dagger}{\partial\phi^2} + 2U\frac{\partial U^\dagger}{\partial\phi}\frac{\partial}{\partial\phi}. \tag{4.2.11}$$

Equation (4.2.11) does not immediately look Hermitian, but it can be rewritten by decomposing the last term into a Hermitian and an anti-Hermitian part. We use the fact that two operators A and B can be decomposed into a Hermitian and anti-Hermitian part as follows,

$$AB = \frac{1}{2}(AB + B^\dagger A^\dagger) + \frac{1}{2}(AB - B^\dagger A^\dagger). \tag{4.2.12}$$

Using this equation we can rewrite Equation (4.2.11) to be,

$$H = \frac{\partial^2}{\partial\phi^2} + U\left(\frac{\partial^2 U^\dagger}{\partial\phi^2}\right) + \left(U\frac{\partial U^\dagger}{\partial\phi}\frac{\partial}{\partial\phi} + \frac{\partial}{\partial\phi}U\frac{\partial U^\dagger}{\partial\phi}\right) + \left(U\frac{\partial U^\dagger}{\partial\phi}\frac{\partial}{\partial\phi} - \frac{\partial}{\partial\phi}U\frac{\partial U^\dagger}{\partial\phi}\right) \tag{4.2.13}$$

$$= \frac{\partial^2}{\partial\phi^2} + U\left(\frac{\partial^2 U^\dagger}{\partial\phi^2}\right) + \left(U\frac{\partial U^\dagger}{\partial\phi}\frac{\partial}{\partial\phi} + \frac{\partial}{\partial\phi}U\frac{\partial U^\dagger}{\partial\phi}\right) + U\frac{\partial U^\dagger}{\partial\phi}\frac{\partial}{\partial\phi} - \frac{\partial U}{\partial\phi}\frac{\partial U^\dagger}{\partial\phi} - U\frac{\partial^2 U^\dagger}{\partial\phi^2} - U\frac{\partial U^\dagger}{\partial\phi}\frac{\partial}{\partial\phi} \tag{4.2.14}$$

$$= \frac{\partial^2}{\partial\phi^2} + \left(U\frac{\partial U^\dagger}{\partial\phi}\frac{\partial}{\partial\phi} + \frac{\partial}{\partial\phi}U\frac{\partial U^\dagger}{\partial\phi}\right) - \frac{\partial U}{\partial\phi}\frac{\partial U^\dagger}{\partial\phi}. \tag{4.2.15}$$

Here the first and the last term are clearly Hermitian and the middle term is Hermitian by construction. Now that we have the Averin Hamiltonian in the basis of the Beenakker Hamiltonian we calculate $\partial U^\dagger/\partial\phi$ using Equation (4.2.4).

$$\frac{\partial U^\dagger}{\partial\phi} = \frac{\partial}{\partial\phi}e^{-i\sigma_2 y} = e^{-i\sigma_2 y}\left(-i\sigma_2\frac{\partial y}{\partial\phi}\right) = U^\dagger\left(-i\sigma_2\frac{\partial y}{\partial\phi}\right). \tag{4.2.16}$$

With these equations we can now write the full Averin Hamiltonian in the basis of Beenakker's Hamiltonian by inserting Equation (4.2.16) into (4.2.15) and adding

in the transformed potential which by construction is Beenakker's potential.

$$H_A = E_C\sigma_0\frac{\partial^2}{\partial\phi^2} + \Delta\sigma_3\sqrt{1 - T\sin\left(\frac{\phi}{2}\right)^2} \underbrace{- E_C\sigma_0\left(\frac{\partial y}{\partial\phi}\right)^2 - E_C\sigma_2\left(i\frac{\partial}{\partial\phi}\left(\frac{\partial y}{\partial\phi}\right) + \left(\frac{\partial y}{\partial\phi}\right)i\frac{\partial}{\partial\phi}\right)}_{\text{Difference from Beenakker}}, \quad (4.2.17)$$

where we have used the fact that $\sigma_2^2 = \sigma_0$. The derivative of $y(\phi)$ is,

$$\frac{\partial y}{\partial\phi} = \frac{\sqrt{1-T}}{4\left(1 - T\sin\left(\frac{\phi}{2}\right)^2\right)}. \quad (4.2.18)$$

Here we can see that if $T = 1$ the there is no difference between Averin and Beenakker as we would expect. In the $T = 0$ limit the derivative reduces to $1/4$ and writing the derivatives in charge basis, so $i\partial/\partial\phi \to n$, the part that separates Averin and Beenakker can be written as,

$$H_{\text{diff.}} = \begin{pmatrix} 1/16 & -i/4\cdot n \\ i/4\cdot n & 1/16 \end{pmatrix} \quad \text{for} \quad T = 0. \quad (4.2.19)$$

Unfortunately this theoretical work does not really tell us much. Equation (4.2.19) would be significantly more helpful if we had an analytical expression for the wavefunctions for either Averin or Beenakker, because then we could operate on that wavefunction and find an approximate expression for energy difference. In this entire calculating we have assumed $n_g = 0$. We could include n_g and we would end some off diagonal term of the form $2n_g i\partial/\partial\phi$. But we would still be stuck with $H_{\text{diff.}}$ not being able to calculate any further.

Chapter 5

Numerics

The Hamiltonians from Beenakker and Averin are not analytically solvable so we have to resort to numerical methods. One of the most straight forward ways of solving differential equations is the finite difference method. The finite difference method takes a partial differential equation (PDE) and turns it into a system of linear equations, which can be written as a matrix and solved on a computer.

5.1 Finite Difference Methode

We solve the time-independent Schrödinger equation by using the finite difference method similarly to Aumann et al.[13]. In the finite difference method the variables, for example space or time, are discretised $x \to [x_0, x_1, ..., x_N]$, where there is a finite difference between each point $x_1 - x_0 = \delta$. The interval over which the PDE is solved should be such that at the cut-off values x_0 and x_N, the solution is essentially zero. The closer it is to zero, the less we loss from truncating the space over which we solve the PDE. The cut-off value depends on the parameters of the differential equation, as they control how spread out the solution is, but the number of solutions of interest also plays a role. For many systems the solution with the lowest eigenvalue is well localised in a minima and solutions with larger eigenvalues will be more spread out. So if we are only interested in the solution with the lowest eigenvalue then we might be able to choose a smaller cut-off value than if we are interested in the lowest 15 solutions.

Another consideration is that the distance between points should not be so big that any important detail is lost. So when we solve our differential equations we have two parameters that we need to keep in mind if we want accurate solutions, the cut-off values and the resolution. But there is no equation to determine what resolution and cut-off value we need to choose. We just have to try a couple of times until we find some values that ensures that the solutions converge.

Once we have discretised the space we need to find out how to represent the derivatives. This can be done by taking the definition of the derivative and taking the limit to δ instead of 0.

$$\frac{\partial f(x_0)}{\partial x} = \lim_{h \to \delta} \frac{f(x_0 + h) - f(x_0)}{h} \Rightarrow \frac{\partial f_n}{\partial x} = \frac{f_{n+1} - f_n}{\delta}, \tag{5.1.1}$$

where f_n is the function value at x_n. This first order approximation of the derivative will run into a problem with extrema. If it is at a perfect extrema where $f_{n+1} = f_{n-1} \neq f_n$ then it will not equal zero as we would expect. To fix this we can make it balanced, as opposed to being biased to the right as it is right now. To make it balanced we take the points on either side of the one where the derivative is acting and increase the denominator to be 2δ to reflect the new distance between the chosen points. So the first derivative becomes,

$$\frac{\partial f_n}{\partial x} = \frac{f_{n+1} - f_{n-1}}{2\delta}. \tag{5.1.2}$$

A similar calculation can be done for the second derivative and we find that,

$$\frac{\partial^2 f_n}{\partial x^2} = \frac{f_{n+1} - 2f_n + f_{n-1}}{\delta^2}. \tag{5.1.3}$$

If we write the function as a vector $f(x) \to = [f_0, f_1, ..., f_N]^T$ the derivatives can be written as matrices,

$$\frac{\partial}{\partial x} = \frac{1}{2\delta}\begin{pmatrix} 0 & 1 & & \\ -1 & 0 & 1 & \\ & -1 & 0 & 1 \\ & & -1 & 0 \end{pmatrix} \quad \text{and} \quad \frac{\partial^2}{\partial x^2} = \frac{1}{\delta^2}\begin{pmatrix} -2 & 1 & & \\ 1 & -2 & 1 & \\ & 1 & -2 & 1 \\ & & 1 & -2 \end{pmatrix}. \tag{5.1.4}$$

Here we have not dealt with the boundary conditions and naively cut of any values outside $[x_0, x_N]$. In our case with ϕ being a 2π periodic variable we need periodic boundary conditions. Using periodic boundary condition allows us to not worry about cut-off values because our coordinate does not go from $-\infty$ to ∞, it is only defined on $[0, 2\pi]$ and loops back on itself. So now we only have to worry about the resolution. We implement this by taking mod$N$ of all the indices (which is the discretised version of taking mod2π). The first derivatives at the ends then become,

$$\frac{\partial f_N}{\partial x} = \frac{f_{N+1} - f_{N-1}}{2\delta} \Rightarrow \frac{f_0 - f_{N-1}}{2\delta} \quad \text{and} \quad \frac{\partial f_0}{\partial x} = \frac{f_{-1} - f_1}{2\delta} \Rightarrow \frac{f_N - f_1}{2\delta}, \tag{5.1.5}$$

and likewise for the second derivative. The derivatives with periodic boundary conditions in matrix form are,

$$\frac{\partial}{\partial \phi} = \frac{1}{2\delta}\begin{pmatrix} 0 & 1 & & -1 \\ -1 & 0 & 1 & \\ & -1 & 0 & 1 \\ 1 & & -1 & 0 \end{pmatrix} \quad \text{and} \quad \frac{\partial^2}{\partial \phi^2} = \frac{1}{\delta^2}\begin{pmatrix} -2 & 1 & & 1 \\ 1 & -2 & 1 & \\ & 1 & -2 & 1 \\ 1 & & 1 & -2 \end{pmatrix}. \tag{5.1.6}$$

We can now discretise the entire Hamiltonian. Take for example the transmon Hamiltonian in flux basis,

$$\left[4E_C \frac{\partial^2}{\partial \phi^2} - E_J \cos(\phi)\right] \Psi = E\Psi, \tag{5.1.7}$$

where the $\cos(\phi)$ operator is,

$$\cos(\phi) \Rightarrow \begin{pmatrix} \cos(\phi_0) & & & & \\ & \cos(\phi_1) & & & \\ & & \ddots & & \\ & & & \cos(\phi_{N-1}) & \\ & & & & \cos(\phi_N) \end{pmatrix}. \tag{5.1.8}$$

Now finding the the wavefunctions and the energies are as simple as finding the eigenvectors and eigenvalues of the matrix inside the brackets in Equation (5.1.7).

5.1.1 Basis switch

When solving Hamiltonians, the initial basis that it is given in, might not be the most efficient way to solve it. Generally if we can choose a basis where the matrix has a lot of zeros in it will becomes easier and quicker to solve. In our case with superconducting qubits we can either use flux basis where our principle variable is ϕ or charge basis where our principle variable is n. Often the Hamiltonians are written in the ϕ basis because non-linear capacitors are rarely used in superconducting qubits, but they do exist[24]. This means that all the capacitors are linear capacitors with n^2 terms. The n^2 terms become second derivatives in the flux basis. So now the Hamiltonian contains a second derivative that looks like the kinetic energy and some other terms that look like a potential. This gives us an intuitive way to think about the system, but this might not be the best way of solving it.

In flux basis we have periodic boundary conditions so we only need to worry about the resolution. We do not have that in charge basis where n goes from $-\infty$ to ∞ so we have to choose appropriate cut-off values. But because flux is a compact variable then the conjugate variable is discretised. So the charge basis can only take specific values. This means that we do not have to worry about making the spacing between points as small as possible because we know the exact spacing. In this case the spacing is 1. So in one basis we only need to worry about the resolution being small enough that we do not loss detail and in the other we only need to worry about the cut-off value and how much of the wavefunction we are throwing away.

If we want to solve the Hamiltonians in charge basis we need to transform the $\cos(\phi)$ operator into charge basis. We do this by inserting the identity $\mathbb{1} = 1/2\pi \int_{-\pi}^{\pi} d\phi \, |\phi\rangle\langle\phi|$ and integrating out ϕ,

$$\begin{aligned} \langle n|\cos(\phi)|m\rangle =& \frac{1}{2\pi} \int_{-\pi}^{\pi} d\phi \, \langle n|\phi\rangle \cos(\phi) \, \langle\phi|m\rangle & (5.1.9) \\ =& \frac{1}{2\pi}\frac{1}{2} \int_{-\pi}^{\pi} d\phi \left(e^{i(m-n+1)\phi} + e^{i(m-n-1)\phi}\right) & (5.1.10) \\ =& -\frac{1}{2\pi}\left(\frac{\sin((m-n)\pi)}{m-n+1} + \frac{\sin((m-n)\pi)}{m-n-1}\right) & (5.1.11) \\ =& \frac{1}{2}\delta_{m,n\pm1} \quad \text{for} \quad m,n \in \mathbb{Z} & (5.1.12) \end{aligned}$$

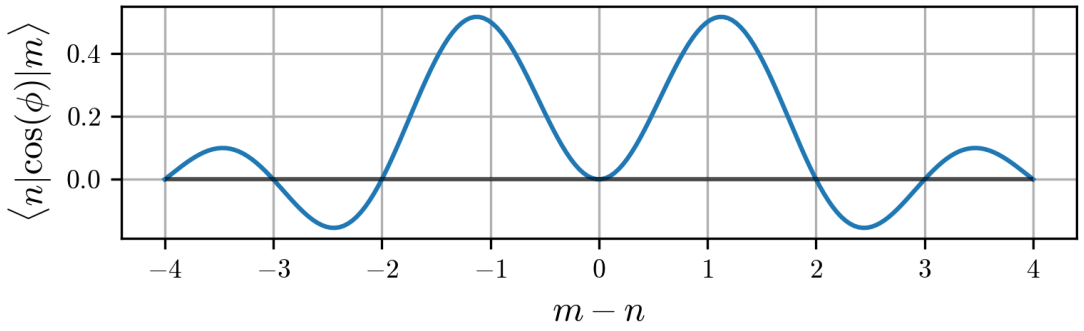

Figure 5.1: The $\cos(\phi)$ operator in charge basis. The function plotted is Equation (5.1.11). Here we can see that the only non-zero integer values are ± 1.

The reason the last equality holds is that $\sin(\pi k) = 0$ for $k \in \mathbb{Z}$, but at $m-n = \pm 1$ we have a zero divided by zero expressions. Evaluating Equation (5.1.11) in the limits $m - n = 1$ and $m - n = -1$ we find that they are both $1/2$. Using the fact that m and n can only be integers the $\cos(\phi)$ operator only has non-zero values on the longest off diagonals,

$$\cos(\phi) \Rightarrow \frac{1}{2}\begin{pmatrix} 0 & 1 & & & \\ 1 & 0 & 1 & & \\ & \ddots & & & \\ & & 1 & 0 & 1 \\ & & & 1 & 0 \end{pmatrix}. \tag{5.1.13}$$

We can also transform $\cos(\phi/2)$ into charge basis,

$$\begin{aligned} \langle n|\cos(\phi/2)|m\rangle =& \frac{1}{2\pi}\int_{-\pi}^{\pi} d\phi \, \langle n|\phi\rangle \cos(\phi/2) \langle \phi|m\rangle & (5.1.14)\\ =& \frac{1}{2\pi}\frac{1}{2}\left[\int_{-\pi}^{\pi} d\phi e^{i(m-n+1/2)\phi} + \int_{-\pi}^{\pi} d\phi e^{i(m-n-1/2)\phi}\right] & (5.1.15)\\ =& \frac{1}{4\pi}\left(\frac{e^{i(m-n)\pi} + e^{-i(m-n)\pi}}{m-n+1/2} + \frac{-e^{i(m-n)\pi} - e^{-i(m-n)\pi}}{m-n-1/2}\right) & (5.1.16)\\ =& \frac{1}{4\pi} 2\cos(\pi(m-n))\left(\frac{1}{m-n+1/2} - \frac{1}{m-n-1/2}\right) & (5.1.17)\\ =& -\frac{2\cos(\pi(m-n))}{\pi(4(m-n)^2-1)}. & (5.1.18) \end{aligned}$$

A similar calculation can be carried out for $\sin(\phi/2)$ where we find that,

$$\langle n|\sin(\phi/2)|m\rangle = -\frac{4i(m-n)\cos(\pi(m-n))}{\pi(4(m-n)^2-1)}. \tag{5.1.19}$$

5.2 Convergence

5.2.1 Basis dependent convergence

Before we start investigating the behaviour of the Hamiltonians we will figure out what basis is the most efficient to work in, because down the line some of these matrices had the possibility of getting very big. This turned out to be less of a concern after we found out that we would not be able to extend Averin's Hamiltonian into the multichannel regime as discussed in Section 3.2. But there is still value in implementing the Hamiltonians in both bases. The reason is that implementing the system in both bases we can check whether or not they converge to the same values. If they converge to the same values it is a strong indication that we have implemented them correctly.

The first Hamiltonian that we implemented was the transmon[1]. The most important thing when choosing a resolution to work with is that all the values of interest have converged to their final value. So plotting the 4 lowest eigenvalues as a function of the resolution we can find out how low we need the spacing to be for the eigenvalues to converge. In Figure 5.2 we can see the difference in convergence between the two bases. In Figure 5.2b we see that the eigenvalues converge at matrices of size 12 to 15 and that it takes around a millisecond to calculate. From this figure we can also see the fact that the lower eigenvalues converge faster then the higher ones. These calculation time will vary from computer to computer so the absolute time is not very useful. They can only tell us something when compared to other computational times on the same computer.

On the other hand, in Figure 5.2a we see that for the lowest 3 eigenvalues we need a resolution of 20 to 25 and if we want to calculate the 4^{th} eigenvalue as well, we need a resolution of around 30 and the computational time becomes 3-4 millisecond. So for the transmon charge basis is the most efficient basis because we can use matrices half the size and the computation takes one fourth of the time compared to using the flux basis.

We can make a similar plot for the gatemon solving Averin's Hamiltonian. We have not implemented Beenakker's Hamiltonian in charge basis because if T is not 1 or 0 then the basis change is an elliptic integral which does not have an analytical solution and then we would have to do element wise numerical integration to do the change of basis. This would be too computationally intensive and we would loose the potential advantage of switching bases. Figure 5.3 is similar to Figure 5.2 but the x-axis is the resolution of the $\cos(\phi/2)$ and $\sin(\phi/2)$ matrices so the full matrix being solved is twice as big. The reason for that is that (3.2.4) can be written as,

$$\hat{H}_A = 4E_C(\hat{n} - n_g)^2 \otimes \hat{I}_2 + \Delta\left[\cos(\phi/2) \otimes \sigma_3 + \sin(\phi/2) \otimes \sigma_2\right], \tag{5.2.1}$$

where σ_2 and σ_3 are the Pauli matrices. In charge basis the cut-off values have to be so large that the wavefunction is essentially zero at that point, so we loose as

[1]Github repository where the code to generate the plots is stored: https://github.com/Shellf1sh/Speciale

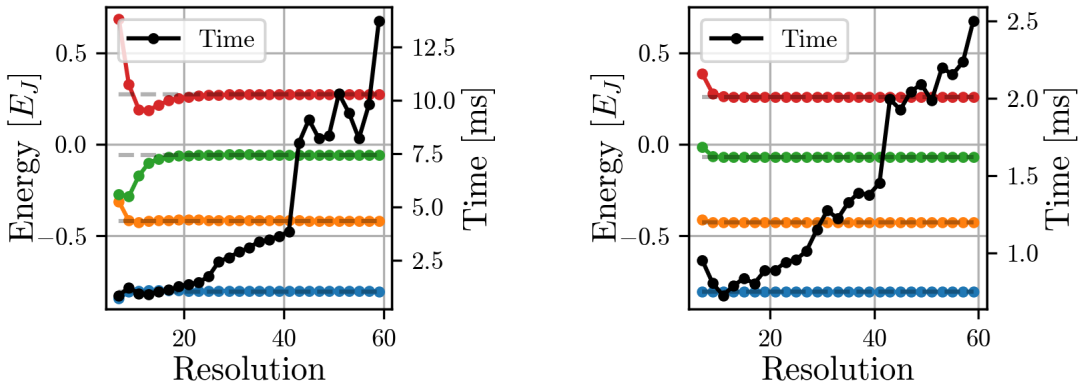

(a) Flux basis

(b) Charge basis

Figure 5.2: Convergence of the 4 lowest eigenvalues for the transmon(2.2.5) at different computational resolutions with $E_J/E_C = 50$ and $n_g = 0$. The grey dashed line is the value of the last point (i.e. the highest resolution). **(a)** Transmon in flux basis. Since the flux is periodic, the resolution n corresponds to a spacing between points which is $2\pi/n$. **(b)** Transmon in charge basis. Because the spacing is exact in charge basis a resolution of n corresponds to a cut-off value of $(n-1)/2$(We only solve for n odd so that it is symmetric around 0.).

little information as possible by truncating the calculation. This means that in the very heavy limit we can run into problems with the charge basis. The reason for that, is in the heavy limit the system is narrowly localised in flux space, but that means that it is almost completely delocalised in charge space due to the fact that Fourier transforming a narrow function from one space creates a wide function in the conjugate space. An extreme example of this is that the Fourier transform of the delta function is the constant function, the narrowest possible function Fourier transforms into the widest possible function. This means that the wavefunction will not go to zero before the cut off value and then the solutions cannot be trusted. One might think that we would then get the same problem with the flux basis in the very light limit, because there it is opposite. The wavefunction is localised in number space, but delocalised in ϕ space. But this delocalisation does not cause a problem because in the flux basis we have periodic boundary conditions so it is not am issue that the wavefunction extends all the way to boundary.

In Figure 5.3 we see charge basis is still the most efficient basis to solve the Hamiltonian because we do not need as big of a matrix for convergence of the solutions. But compared to Figure 5.2, we see that in 5.3, for similar sized matrices flux basis is now more efficient. The reason is that the Fourier transform of the $\cos(\phi/2)$ and $\sin(\phi/2)$ matrices are not mostly zero. Equation (5.1.18) and (5.1.19) do not have a lot of zero like (5.1.11). This means that we loss the advantage of using numerical methods like `scipy.sparse` in Python that are specifically design to work effectively on sparse matrices (matrices that contain mostly zeros).

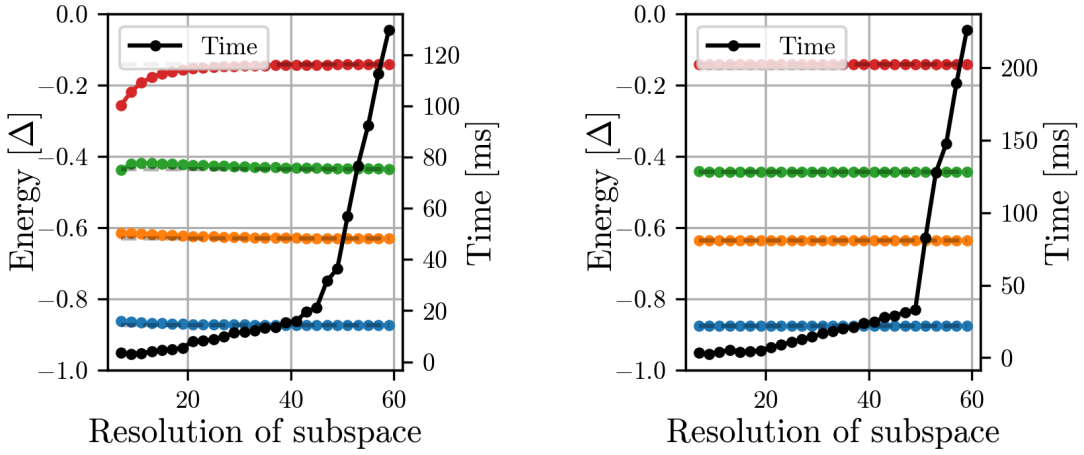

(a) Flux basis

(b) Charge basis

Figure 5.3: The 4 lowest eigenvalues for Averin's Hamiltonian(3.2.4) at different computational resolutions with $\beta = 5$, $n_g = 0$ and $T = 0.8$. The grey dashed line is the value of the last point (i.e. the highest resolution). **(a)** Gatemon in flux basis. Since the flux is periodic the resolution n corresponds to a spacing between points the is $2\pi/n$. **(b)** Gatemon in charge basis. Because the spacing is exact in charge basis a resolution of n corresponds to a cut-off value of $(n-1)/2$(We only solve for n odd so that it is symmetric around 0.).

5.2.2 Scaling

Now that we have chosen the appropriate size and basis to solve our Hamiltonian we can now compare models. When we want to compare models we need to scale them correctly so that we can see where they are different and where they for all practical purposes are the same. The transmon has one characteristic parameter, the energy ratio E_J/E_C. We will define this parameter to be β. Using that and rescaling the transmon Hamiltonian (2.2.5) it can be written as,

$$H_T = 4\frac{1}{\beta}(n - n_g)^2 - \cos(\phi). \tag{5.2.2}$$

Now the energy is scaled to the depth of the potential. We will also rewrite Beenakker's Hamiltonian to be scale to the depth of the potential. We do this by using the Taylor expansion from Section 4.1.2 so Equation (3.1.11) becomes,

$$H_B \approx 4E_C(n - n_g)^2 - \frac{\Delta T}{4}\cos(\phi) - \Delta\left(1 - \frac{T}{4}\right). \tag{5.2.3}$$

In this Hamiltonian $\Delta T/4$ is the effective Josephson energy $\tilde{E}_J$. That means that for Beenakker's Hamiltonian $\beta = \tilde{E}_J/E_C = \Delta T/4E_C$. We then use this to insert $E_C = \Delta T/4\beta$,

$$H_B \approx 4\frac{\Delta T}{4\beta}(n - n_g)^2 - \frac{\Delta T}{4}\cos(\phi) - \Delta\left(1 - \frac{T}{4}\right). \tag{5.2.4}$$

In Equation (5.2.2) the prefactor in the cosine term is 1. So the get the Hamiltonians on the same energy scale we multiply Equation (5.2.4) with $4/\Delta T$.

$$H_B \approx 4\frac{1}{\beta}(n-n_g)^2 - \cos(\phi) - \frac{4}{T}\left(1-\frac{T}{4}\right). \tag{5.2.5}$$

When we now compare the transmon and Beenakker's model they will agree in the low transmission limit as we would physically expect. As we increase T we can see how they differ. With this scaling and correction Beenakker's Hamiltonian becomes,

$$H_B = 4\frac{1}{\beta}(n-n_g)^2 - \frac{4}{T}\sqrt{1-T\sin(\phi/2)^2} + \frac{4}{T}\left(1-\frac{T}{4}\right). \tag{5.2.6}$$

This version of Beenakker's Hamiltonian will give the same results as the transmon in the small T limit. We also apply this scaling to Averin's Hamiltonian so that Beenakker and Averin agree at $T = 1$.

5.2.3 Comparison

Now we are in a situation where we can compare the Hamiltonians on similar energy scales to see how they differ. The first comparison we do is to plot the the two different gatemon models and the transmon with the same β, on the same energy scale and vary T.

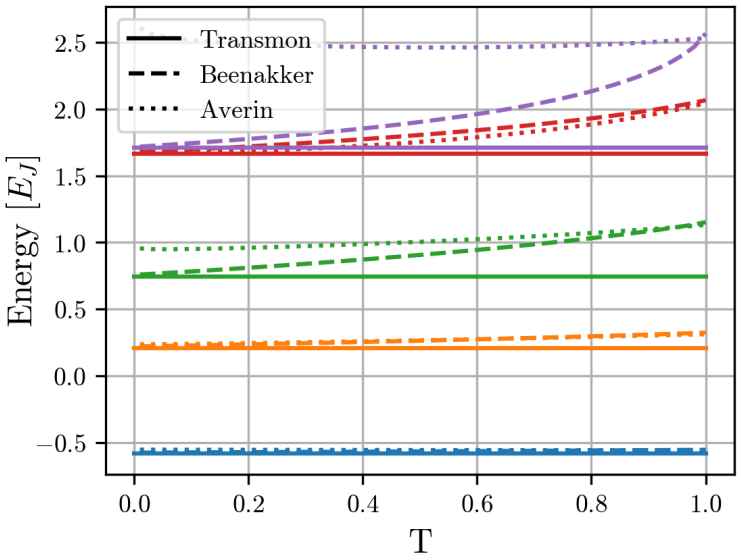

Figure 5.4: The eigenvalues of the three different models with $\beta = 10$. The transmon is flat because T does not appear in the transmon Hamiltonian.

In Figure 5.4 we can see that in the small T limit, the transmon and Beenakker's Hamiltonian agree as we have scaled them to do. In the high T limit we see that Averin and Beenakker agree. This is because for $T = 1$ then $r = 0$ and the

two subspaces in Averin's Hamiltonian decouple and become the two solutions of Beenakker's Hamiltonian we saw in Section 4.1.2. So Figure 5.4 makes sense insofar as the limits are what we expect them to be. This together with the convergence of eigenvalues in Section 5.2.1 is strong evidence that the numerical methods have been implemented correctly.

The apparent degeneracy in the transmon model comes from the fact that for states with high energy the potential is just a small perturbation, so they are essentially free particles with periodic boundary conditions. This system is "the particle on a ring" and its states are double degenerate except for the ground state. The Hamiltonian for the particle on a ring is,

$$H_{ring}\Psi = -\frac{\hbar^2}{2m}\frac{\partial^2\Psi}{\partial\phi^2} = E\Psi \quad \text{with} \quad \Psi(0) = \Psi(L), \tag{5.2.7}$$

where L is the circumference of the ring. The solution to this Hamiltonian is the complex exponential,

$$\Psi(\phi) = \exp\left\{ i\frac{\sqrt{2mE}}{\hbar}\phi \right\}. \tag{5.2.8}$$

We then have to look at the periodic boundary conditions. $\Psi(0) = 1$ so therefore $\Psi(L) = 1$ which means that $L\sqrt{2mE}/\hbar = n\pi$ where $n \in \mathbb{Z}$. Rearranging, the energy of the states are,

$$E = \frac{\pi^2}{2mL^2}n^2, \tag{5.2.9}$$

which is doubly degenerate except for all n except $n = 0$, which is the unique ground state. This is why we see that the transmon is almost degenerate for high energy, and the splitting gets smaller the higher in energy we go.

Another way to illustrate this is to make a plot where we keep T constant and then vary β. In Figure 5.5 we have the three lowest eigenvalues as a function of β for four different transmissions. The first thing to note here is that for the top plots where T is small we see that the transmon (filled line) and Beenakker's Hamiltonian (dashed line) agree at all weights as predicted in Section 4.1.2.

We also see that in all cases when the energies rise in the low β limit, the first and second excited states converge to the same value for the transmon and Beenakker. This is consistent with the particle on a ring model in the light regime. Also the ground state goes to zero which again is consistent with Equation (5.2.9). This is because lowering β increases the kinetic energy while keeping the potential energy constant. That is equivalent to keeping the kinetic energy constant and lowering the potential energy and as the potential energy gets smaller and smaller the system becomes more like a particle on a ring.

A third thing which we see from the inserts in Figure 5.5 is that the in the heavy limit, for all T, Beenakker's Hamiltonian and Averin's Hamiltonian agree as predicted in Section 4.1.1. We see in Figure 5.5 that everything is well behaved and gives the predicted behaviour. So this is another good indication, on top of the convergence in different bases in Section 5.2.1 that the numerical implementation is correct.

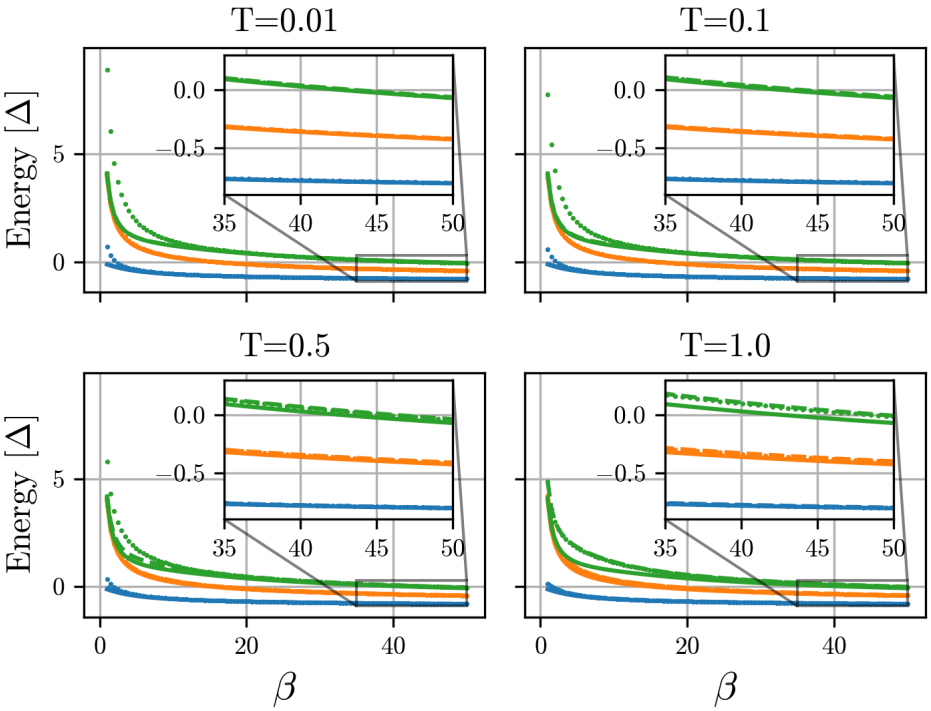

Figure 5.5: The eigenvalues of the three different models at four different transmission. The filled line is the transmon, the dashed line is Beenakker and the dotted line is Averin. E_0=blue, E_1=orange and E_2=green.

5.3 Multichannel Beenakker

So far we have been solving Beenakker's Hamiltonian with only one channel. But there is nothing stopping us from solving it with more channels. In the flux basis, which is the only one available to us for Beenakker's Hamiltonian, the potential term is diagonal so the discretisation is straight forward. In Figure 5.6 we have plotted the qubit frequency of Beenakker's Hamiltonian with four channels as they progressively open up.

This smaller and smaller increase in qubit frequency can be explained by using some of the same approximation that are used with the transmon. To justify this we use that in the heavy limit the system is similar to the transmon in the fact that it is a weakly anharmonic oscillator. Bearing this in mind we will use the same approximation for the qubit frequency that Koch et al. uses[14]. By taking the transmon as a weakly anharmonic oscillator and then expanding the $\cos(\phi)$ term to 4^{th} order in ϕ they get a Duffing oscillator which they use to calculate the correction to the harmonic oscillator energies. Using that they find that $\omega_q \propto \sqrt{E_C E_J}$. For every open channel we add the effective E_J increases by $\approx \Delta$ so for the multichannel Beenakker Hamiltonian in the heavy limit $\omega_q \propto \sqrt{N}$ where N is the number of open channels, which is why we see a smaller and smaller increase in qubit frequency in Figure 5.6 for every channel we open up.

One of the challenges of characterising the gatemon is that we do not actually

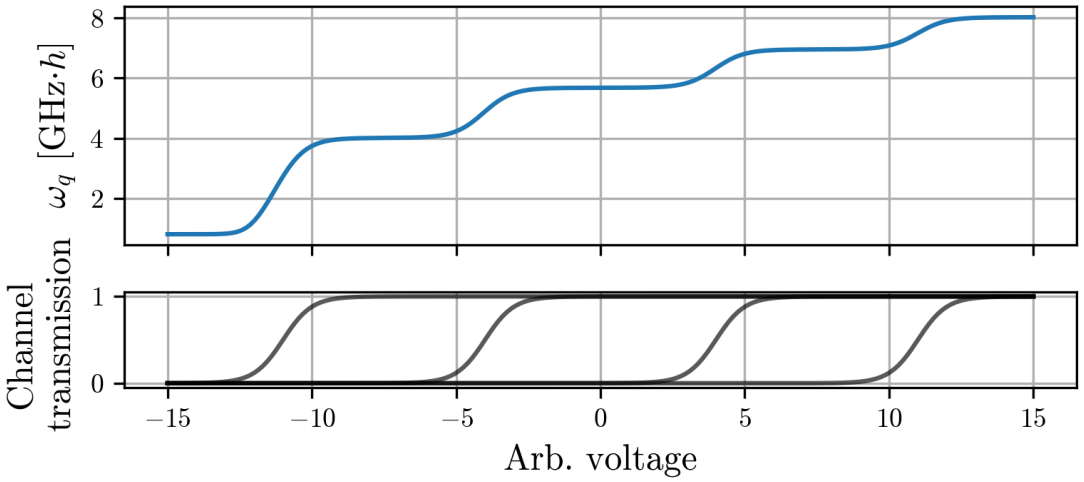

Figure 5.6: Along the x-axis is an arbitrary voltage which is supplied through the drive line. As this voltage is changed more channels will open up. In the top plot the qubit frequency is plotted as a function of the voltage as these channels open.

know how many channels are open. At a given voltage it will vary between samples as it is highly dependent on specific structure of the sample such as impurities and domain walls. It is not impossible to figure out how many channels are how open, it is just very hard to do on the gatemon circuit. Hart et al.[25] managed to characterise a nanowire by using a aluminium ring with a part of it cut out and replaced by the nanowire. They then had another loop above it to measure the magnetic flux and a third ring to induce an external magnetic field. They did this because knowing the magnetic flux they can find the super current. From Beenakker[19] they have the super current as a function of the change in density of states with respect to the superconducting phase,

$$I = -\frac{2e}{\hbar} 2k_B T \int_{\Delta_0}^{\infty} d\varepsilon \ln(2\cosh(\varepsilon/2k_B T)) \frac{\partial \rho}{\partial \phi}. \tag{5.3.1}$$

The density of states can be found from,

$$\rho = \frac{1}{2\pi i} \frac{\partial}{\partial E} \mathrm{Tr}\{\ln(S)\} = \frac{1}{2\pi i} \frac{\partial}{\partial E} \ln(\det\{S\}). \tag{5.3.2}$$

The derivation of this equation can be found in appendix A. They then simplify the expression so they get,

$$I(\phi) = -\frac{2e}{\hbar} \sin(\phi) \sum_{p=1}^{N} \frac{T_p}{\varepsilon_p} \tanh \frac{\varepsilon_p}{2k_B T}. \tag{5.3.3}$$

They first induced a magnetic field with the third ring. This magnetic field threaded the ring with the nanowire on and tuned the phase difference ϕ. That then generated a super current that induced a new magnetic field that the second ring could be measured. With the phase-current relation measured they then fit

Equation (5.3.3) to the measured phase-current relation with the T_p's as parameters. This works when the nanowire is not used for anything else, but the extra rings and the loop with the nanowire are not feasible to do on the gatemon circuit. So because we do not know how many channels there are and we have found no fundamental difference in the dynamics when adding the the extra channels when calculating the T_1 times in Section 6 then we will just use one channel. This also enables a more one to one comparison with Averin's Hamiltonian.

Chapter 6

Noise

In real systems there will be unpredictable interactions with the environment that will affect the system. These effects will introduce noise into the system. In qubits this noise is detrimental to the lifetime of the qubit because these noise fluctuations will cause stimulated emission and increase the decay rate of the qubit. Noise can be categorised into different types. Some of the most pervasive and common types of noise that will be the focus of this thesis are $1/f$ noise and ohmic noise.

6.1 Ohmic

Our qubit can unfortunately not be completely isolated from the environment. There is a continuum of states in the environment that it couples to, and that reduces our coherence time. So now we need to find the spectral density that describes this coupling. The spectral density is defined as[26],

$$S_f(\omega) = 2\pi\hbar \sum_{\alpha,\gamma} \rho_{\alpha\alpha} |\langle\alpha|f|\gamma\rangle|^2 \delta(\varepsilon_\gamma - \varepsilon_\alpha - \hbar\omega), \tag{6.1.1}$$

where f is the operator responsible for the noise and ρ is the density matrix. The way we will model it is as if the qubit is capacitively coupled to an infinitely long transmission line. Voltage fluctuations in the end of the transmission line will take the role as voltage fluctuations around the qubit. These fluctuations induce stimulated emission of the qubit and that increases the relaxation rate of the qubit so that excitations can escape through the transmission line and and never return.

The transmission line has inductance l per unit length and capacitance c per unit length. The Lagrangian for the transmission line is[26],

$$\mathcal{L} = \int_0^\infty dx \frac{l}{2} j^2 - \frac{1}{2c} q^2, \tag{6.1.2}$$

where $j(x,t)$, the current density, and $q(x,t)$, the charge density, are functions of time and place and the obey the continuity equation $\partial_x j + \partial_t q = 0$. To make sure that the continuity equation is satisfied, we introduce a new variable θ which we define as,

$$\theta(x,t) = \int_0^x dx' q(x',t). \tag{6.1.3}$$

Then $q(x,t) = \partial_x\theta$ and $j(x,t) = -\partial_t\theta$ will always satisfy the continuity equation. We can then write the Lagrangian as a function of θ,

$$\mathcal{L} = \int_0^\infty dx \frac{l}{2}(\partial_t\theta)^2 - \frac{1}{2c}(\partial_x\theta)^2. \tag{6.1.4}$$

We can then use the Euler-Lagrange equation to get the wave equation,

$$\frac{\partial\mathcal{L}}{\partial\theta} = \frac{\partial}{\partial x}\frac{\partial\mathcal{L}}{\partial(\partial_x\theta)} + \frac{\partial}{\partial t}\frac{\partial\mathcal{L}}{\partial(\partial_t\theta)} \Rightarrow 0 = l\frac{\partial^2\theta}{\partial x^2} - \frac{1}{c}\frac{\partial^2\theta}{\partial t^2}. \tag{6.1.5}$$

For now we make the transmission line a finite length L, later we will extend it to infinity again later. The proper boundary conditions for θ are $\theta(0,t) = \theta(L,t) = 0$. This is because,

$$\theta(0,t) = \int_0^0 dx' q(x',t) = 0 \quad \text{and} \quad \theta(L,t) = \int_0^L dx' q(x',t) = 0. \tag{6.1.6}$$

The transmission line is neutral so the total charge in the line is zero, so the second integral is zero. With these boundary conditions the general solution to the wave equation can be written as a sum of the normal modes[27],

$$\theta(x,t) = \sqrt{\frac{2}{L}}\sum_{n=1}^{\infty}\phi_n(t)\sin(k_n x), \tag{6.1.7}$$

with $k_n = n\pi/L$. We now carry out the integration in Equation (6.1.4) for each of the two terms.

$$\int_0^L dx' \frac{l}{2}\left(\frac{\partial\theta}{\partial t}\right)^2 = \frac{l}{2}\int_0^L dx' \frac{2}{L}\left(\sum_{n=0}^{\infty}\frac{\partial\phi_n}{\partial t}\sin(k_n x')\right)^2 \tag{6.1.8}$$

$$= \frac{l}{2}\frac{2}{L}\int_0^L dx' \left(\sum_{n=1}^{\infty}\left(\frac{\partial\phi_n}{\partial t}\right)^2 \sin(k_n x')^2\right) \tag{6.1.9}$$

$$= \frac{l}{2}\frac{2}{L}\sum_{n=1}^{\infty}\left(\frac{\partial\phi_n}{\partial t}\right)^2 \int_0^L dx' \sin(k_n x')^2 \tag{6.1.10}$$

$$= \frac{l}{2}\frac{2}{L}\sum_{n=1}^{\infty}\dot{\phi_n}^2\left(\frac{L}{2} + \frac{L}{2\pi n}\frac{\sin(2\pi n) - \sin(0)}{2}\right) \tag{6.1.11}$$

$$= \frac{l}{2}\sum_{n=1}^{\infty}\dot{\phi_n}^2. \tag{6.1.12}$$

In Equation (6.1.9) we can move the exponent inside the brackets because the sine functions are an orthonormal basis so any cross term from squaring the sum will vanish once we do the integral. Similarly the second term in Equation (6.1.4)

becomes,

$$\int_0^L dx' \frac{1}{2c}\left(\frac{\partial\theta}{\partial x}\right)^2 = \frac{1}{2c}\int_0^L dx' \frac{2}{L}\left(\sum_{n=1}^{\infty}\phi_n k_n \cos(k_n x')\right)^2 \tag{6.1.13}$$

$$= \frac{1}{2c}\frac{2}{L}\sum_{n=1}^{\infty}\phi_n^2 k_n^2 \int_0^L dx' \cos(k_n x')^2 \tag{6.1.14}$$

$$= \frac{1}{2c}\sum_{n=1}^{\infty} k_n^2\phi_n^2. \tag{6.1.15}$$

Putting Equation (6.1.12) and (6.1.15) into (6.1.4) we find that,

$$\mathcal{L} = \sum_{n=1}^{\infty}\frac{l}{2}\dot{\phi_n}^2 - \frac{1}{2c}k_n^2\phi_n^2 \tag{6.1.16}$$

So now we have rewritten the Lagrangian to be a sum of independent harmonic oscillators. This sum of harmonic oscillators mimic the continuum. If the sum is large enough with many different k_n's then the energy splitting will be so small that it is effectively a continuous spectrum. We find the conjugate variables by doing the Legendre transformation and the Hamiltonian is,

$$H = \sum_{n=1}^{\infty}\frac{1}{2l}p_n^2 + \frac{1}{2c}k_n^2\phi_n^2. \tag{6.1.17}$$

ϕ_n and p_n can be written as raising and lowering operators,

$$\phi_n = \sqrt{\frac{\hbar}{2l\Omega_n}}(a^\dagger + a) \quad \text{and} \quad p_n = i\sqrt{\frac{\hbar l\Omega_n}{2}}(a^\dagger - a) \tag{6.1.18}$$

with $\Omega_n = k_n/\sqrt{lc}$. We know evaluate the voltage at the end of the transmission line, which is what the qubit "sees". First the voltage is given by,

$$V = \frac{q(0,t)}{c} = \frac{1}{c}\frac{\partial\theta(0,t)}{\partial x} = \frac{1}{c}\sqrt{\frac{2}{L}}\sum_{n=1}^{\infty}k_n\phi_n = \frac{1}{c}\sqrt{\frac{2}{L}}\sum_{n=1}^{\infty}k_n\sqrt{\frac{\hbar}{2l\Omega_n}}(a^\dagger + a). \tag{6.1.19}$$

Inserting this into Equation (6.1.1) we get

$$S_V(\omega) = 2\pi\hbar\frac{2}{L}\sum_{n=1}^{\infty}\frac{\hbar\Omega_n}{2c}\frac{\sqrt{lc}}{\hbar} \times \left[\left|\sqrt{n_B(\hbar\Omega_n)+1}\right|^2\delta(\hbar\Omega_n - \hbar\omega) + \left|\sqrt{n_B(\hbar\Omega_n)}\right|^2\delta(\hbar\Omega_n + \hbar\omega)\right], \tag{6.1.20}$$

where, since the transmission line is in thermal equilibrium, the occupation of states is given by the Bose-Einstein distribution n_B. We now make the transmission line infinite again and in that process we can convert the sum to an integral

over k using $2\pi/L\sum \to \int dk$ when $L \to \infty$. We switch variables $dk \to \sqrt{lc}\, d\Omega$ and the delta functions becomes Heaviside functions,

$$S_V(\omega) = 2R_0\hbar\left[\omega(n_B(\hbar\omega)+1)\Theta(\omega) - \omega n_B(-\hbar\omega)\Theta(-\omega)\right], \tag{6.1.21}$$

where $R_0 = \sqrt{l/c}$. The positive and negative frequency parts of this equation can be combined to a simpler expression,

$$-\omega n_B(-\hbar\omega) = \frac{-\omega}{e^{-\frac{\omega\hbar}{k_BT}}-1} = \frac{\omega}{1-e^{-\frac{\omega\hbar}{k_BT}}} \quad \text{for} \quad \omega > 0, \tag{6.1.22}$$

$$\omega(n_B(\hbar\omega)+1) = \omega\frac{e^{\frac{\omega\hbar}{k_BT}}}{e^{-\frac{\omega\hbar}{k_BT}}-1} = \frac{\omega}{1-e^{-\frac{\omega\hbar}{k_BT}}} \quad \text{for} \quad \omega < 0. \tag{6.1.23}$$

The spectral density becomes,

$$S_V(\omega) = \frac{2R_0\hbar\omega}{1-e^{-\frac{\omega\hbar}{k_BT}}}. \tag{6.1.24}$$

We now look at the limits. In the $\hbar\omega \ll k_BT$ we Taylor expand the exponential to first order.

$$\frac{2R_0\hbar\omega}{1-e^{-\frac{\hbar\omega}{k_BT}}} \approx \frac{2R_0\hbar\omega}{1-1+\frac{\hbar\omega}{k_BT}} = 2R_0k_BT. \tag{6.1.25}$$

This is Johnson-Nyquist noise also called thermal noise because it is directly proportional to the temperature. This was first observed by J.B. Johnson and described by H. Nyquist[28, 29]. The other limit $\omega \gg T$ is the one that is relevant for superconducting qubits as they are placed in cryostats. In that case the exponential becomes vanishingly small and the spectral density reduces to,

$$S_V(\omega) = 2R_0\hbar\omega. \tag{6.1.26}$$

This expression is what is called ohmic noise and the model of the continuum as a sum of harmonic oscillators is called an ohmic bath. It as first proposed by Caldeira and Leggett for dissipation in quantum systems[30].

6.2 $1/f$

One of the most universal types of noise is low frequency noise that has the power spectral function $1/f^\alpha$, where α is close to unity (for brevity this kind of noise is called $1/f$ noise even when $\alpha \neq 1$). This kind of noise appears in a surprising amount of different system. It appears in electronic system such as thin metal films, superconductors, semiconductors and MOSFET's but also other types of system such as cells, the cardiovascular system, the neural network of the brain and in the number of daily trades of stocks[31, 32].

An important thing to note about $1/f$ is that the spectrum cannot follow a $1/f$ power law for the entire range of frequencies. If that is the case the spectrum will diverge in either the low or high frequency limit (or in both for α=1). This

would mean that there is infinite energy in the noise which is non-physical. To ensure that the the noise source is physical the power spectrum must go to zero faster than $1/f$ in the high frequency limit and it must diverge slower than $1/f$ in the lower frequency limit such that the total power is finite. But it turns out that for any physically realisable frequencies from 10^{-5}Hz (Which corresponds to over a day. So for most experiments this will simply be a constant offset.)[1] to 10^{23}Hz which is orders of magnitude lower than the time it takes for light to cover the distance of an atom, the total power of the fluctuations in a 50Ω resistor will be around 10^{-5}W[33, 34]. So even if we extend the spectrum to all physical frequencies we can introduce cut off frequencies outside anything measurable to ensure convergence.

$1/f$ spectra can be realised as an emergent phenomenon from the sum of processes with exponential decays if the relaxation rates of these processes are uniformly distributed[35, 36]. A single exponential relaxation process can be written as,

$$N(t) = \begin{cases} N_0 e^{-\lambda t} & \text{for} \quad t > 0 \\ 0 \quad \text{for} \quad t < 0 \end{cases}, \tag{6.2.1}$$

where N_0 is a normalisation constant and λ is the relaxation rate. If this for example is a charge trap, then it will repeatedly trap electrons at different times t_k as electrons move past it. This will happen K times within a given time T. Taking the Fourier transform of all of these processes,

$$\mathcal{F}\left[\sum_k N(t-t_k)\right] = \int_{-\infty}^{\infty} dt N_0 \sum_k e^{-\lambda(t-t_k)} e^{-i\omega t} = \frac{N_0}{\lambda + i\omega} \sum_k e^{i t_k \omega}. \tag{6.2.2}$$

With the Fourier transform we find the power spectral function[37],

$$S(\omega) = \lim_{T\to\infty} \frac{1}{T} \left| \mathcal{F}\left[\sum_k N(t-t_k)\right] \right|^2 = \frac{N_0^2}{\lambda^2 + \omega^2} \lim_{T\to\infty} \frac{1}{T} \sum_{k,k'} e^{i(t_k - t_{k'})\omega}. \tag{6.2.3}$$

The last sum reduces to the number of events K. This is because $\sum_k e^{ikx}$ averages out to zero if the k's are random. Thinking of the geometric interpretation of complex numbers it is the sum of random points on a circle and if we have enough of them the they average out to zero. But in our case $t_k - t_{k'}$ is not completely random. t_k and $t_{k'}$ are the same list of random numbers, so there are K terms where $t_k = t_{k'}$. When $t_k = t_{k'}$ that term in the sum is 1. The rest of the terms are random because when $k \neq k'$ then t_k and $t_{k'}$ are uncorrelated so they cancel out and we are left with the sum $\sum_k^K 1 = K$. K/T is the rate and as $T \to \infty$ this becomes the average rate n. So the power spectral function is,

$$S(\omega) = \frac{N_0^2 n}{\lambda^2 + \omega^2}. \tag{6.2.4}$$

[1] Even if lower the cut off to something like 10^{-12}Hz then it would not make a big difference because the total power goes as $\ln(\omega_{\text{upper}}/\omega_{\text{lower}})$.

If the relaxation rates are randomly distributed we can then find the expectation value by integrating over λ with the appropriate probability density function (PDF). Assuming that the relaxation rates are uniformly distributed between λ_1 and λ_2 the PDF is $P_u(\lambda) = 1/(\lambda_2 - \lambda_1)$. The new power spectral function is then,

$$S(\omega) = \int_{\lambda_1}^{\lambda_2} d\lambda S(\omega) P_U(\lambda) \tag{6.2.5}$$

$$= \frac{N_0^2 n}{\lambda_2 - \lambda_1} \int_{\lambda_1}^{\lambda_2} d\lambda \frac{1}{\lambda^2 + \omega^2} \tag{6.2.6}$$

$$= \frac{N_0^2 n}{\lambda_2 - \lambda_1} \frac{\arctan\left(\frac{\omega}{\lambda_2}\right) - \arctan\left(\frac{\omega}{\lambda_1}\right)}{\omega} \tag{6.2.7}$$

If $\omega \ll \lambda_1$ then $\arctan(\omega/\lambda_1) \approx 0$ and if $\omega \gg \lambda_2$ then $\arctan(\omega/\lambda_2) \approx \pi/2$. So in that case the spectral function reduces to,

$$S(\omega) \approx \frac{N_0^2 n \pi}{2(\lambda_2 - \lambda_1)} \frac{1}{\omega} \quad \text{for} \quad \lambda_1 \gg \omega \gg \lambda_2 \tag{6.2.8}$$

which is the $1/f$ spectrum, but only on the interval $\lambda_1 \gg \omega \gg \lambda_2$ which also solves our problem of divergence because all the Lorentzian have a finite total power, so a average of many Lorentzians will also have a finite total power.

6.3 Relaxation Time

T_1 time is the characteristic time it takes for a qubit to decay from the excited state $|1\rangle$ to the ground state $|0\rangle$. The general way to calculate these T_1 times is to use Fermi's Golden Rule[38].

$$\Gamma_1^\lambda = \frac{1}{\hbar^2} \left| \langle 1 | \partial_\lambda \hat{H} | 0 \rangle \right|^2 S_\lambda(\omega) \tag{6.3.1}$$

where λ is the source of noise, for example charge n_g or flux Φ_{ext}. The $S_\lambda(\omega)$ is the spectral function which depends on what kind of noise it is and what the source of the noise is. That could be either $1/f$, ohmic or something else. To find the total relaxation time we take the inverse of the sum of the relaxation rates $T_1 = (\sum_\lambda \Gamma_1^\lambda)^{-1}$. The spectral functions which we derived in Section 6.1 and 6.2 can be written as [38],

$$S_\lambda^{1/f}(\omega) = \frac{2\pi A_\lambda^2 \text{Hz}}{|\omega|}, \qquad S_\lambda^{\Omega}(\omega) = \frac{B_\lambda^2 \omega}{2\pi \cdot 1\text{GHz}}, \tag{6.3.2}$$

where all the constants have been collected into one constant that can be experimentally determined. The commonly used litterateur values for these constants are $A_{n_g} = 10^{-4} e/\sqrt{\text{Hz}}$ and $B_{n_g} = 5.2 \cdot 10^{-9} e/\sqrt{\text{Hz}}$[38–41]. These might be slightly different in different devices, but we will assume that they are close enough that we can use the same constants for both transmons and gatemons. In general there

will be several sources of noise, for example charge noise or flux noise which are the two most common. Flux noise is a concern in circuits where a persistent current can flow. In our circuits that is not the case because of the capacitor where current cannot flow across. In for example a flux-tunable transmon a persistent current can flow around the SQUID so fluctuations in the magnetic field will affect the current and therefore the qubit frequency.

For charge noise the operator in Equation (6.3.1) is the same for all three Hamiltonians (apart from a $\otimes I_2$ which we will suppress here for ease of notation).

$$\frac{\partial H}{\partial n_g} = 8E_C(\hat{n} - n_g) \tag{6.3.3}$$

There are a lot of constants that can be collected in these formulas. The first thing to note is that in the numerical solutions all the energies are in units of GHz$\hbar$. We then define $\tilde{E_C} = E_C \cdot 10^{-9}/\hbar$ where $\tilde{E_C}$ is the capacitive energy in units of GHz.

Starting with $1/f$ charge noise we insert the constants and Equation (6.3.3) into Equation (6.3.1),

$$\Gamma^{1/f}_{n_g} = \frac{1}{\hbar^2}\left|\left\langle 1\right|-\frac{8E_C}{2e}(\hat{n}-n_g)\left|0\right\rangle\right|^2 \frac{2\pi A^2_{n_g}\,\text{Hz}}{|\omega|} \tag{6.3.4}$$

$$= \left|\left\langle 1\right|-8\frac{\tilde{E_C}\cdot 10^{-9}}{2e\hbar}(\hat{n}-n_g)\left|0\right\rangle\right|^2 \frac{2\pi 10^{-8}e^2}{|\omega|} \tag{6.3.5}$$

$$= \frac{2\cdot 64\pi\cdot 10}{4|\tilde{\omega}|}\tilde{E_C}^{\,2}\left|\langle 1|(\hat{n}-n_g)|0\rangle\right|^2, \tag{6.3.6}$$

where $\tilde{\omega}$ is the qubit frequency in GHz. We do a similar calculation for the ohmic noise.

$$\Gamma^{\Omega}_{n_g} = \frac{1}{\hbar^2}\left|\left\langle 1\right|-\frac{8E_C}{2e}(\hat{n}-n_g)\left|0\right\rangle\right|^2 \frac{B^2_{n_g}\tilde{\omega}}{2\pi\cdot 1\text{GHz}} \tag{6.3.7}$$

$$= \left|\left\langle 1\right|8\tilde{E_C}(\hat{n}-n_g)\left|0\right\rangle\right|^2 \frac{10^{18}(5.2\cdot 10^{-9})^2e^2/\text{Hz}}{4e^2\cdot 2\pi}\frac{\tilde{\omega}}{1\text{GHz}} \tag{6.3.8}$$

$$= \frac{(5.2\cdot 8)^2}{4\cdot 2\pi 10^9\text{GHz}}\frac{\tilde{\omega}}{1\text{GHz}}\tilde{E_C}^{\,2}\left|\langle 1|(\hat{n}-n_g)|0\rangle\right|^2. \tag{6.3.9}$$

These are the expressions that we have implemented in code. The reason that they have been rewritten so everything is in gigahertz is that it minimises the chance of rounding errors. When working with computers there is only a finite amount of memory so by using extremely big and very small numbers can give unexpected inaccuracies from rounding errors.

6.4 Results

When calculating the T_1 times we have used a similar scaling as in Section 5.2.3, but instead of starting from E_J we instead start from Δ because it is a material

constant. For aluminium $\Delta \approx 160$meV which converted to gigahertz becomes roughly 40GHz$\hbar$[42]. This means that for Beenakker and Averin $E_C = \Delta/\beta$ and for the transmon $E_J = \Delta T/4$ and $E_C = \Delta T/4\beta$.

In Figure 6.1 the first thing we see is that the heavier circuits have better T_1 times than their light counterparts. This might not necessarily be due to insensitivity to charge noise. That is because the insensitivity to charge noise mainly protects against dephasing. Dephasing will lower the T_2 time of the qubit. This has not been a topic of discussion in this thesis because currently the gatemons being fabricated are T_1 limited, so that is the limiting factor. We also see that the gatemon is limited by ohmic noise. This not a surprise because the gatemon is a high frequency qubit usually designed to operate in the 4-6GHz range.

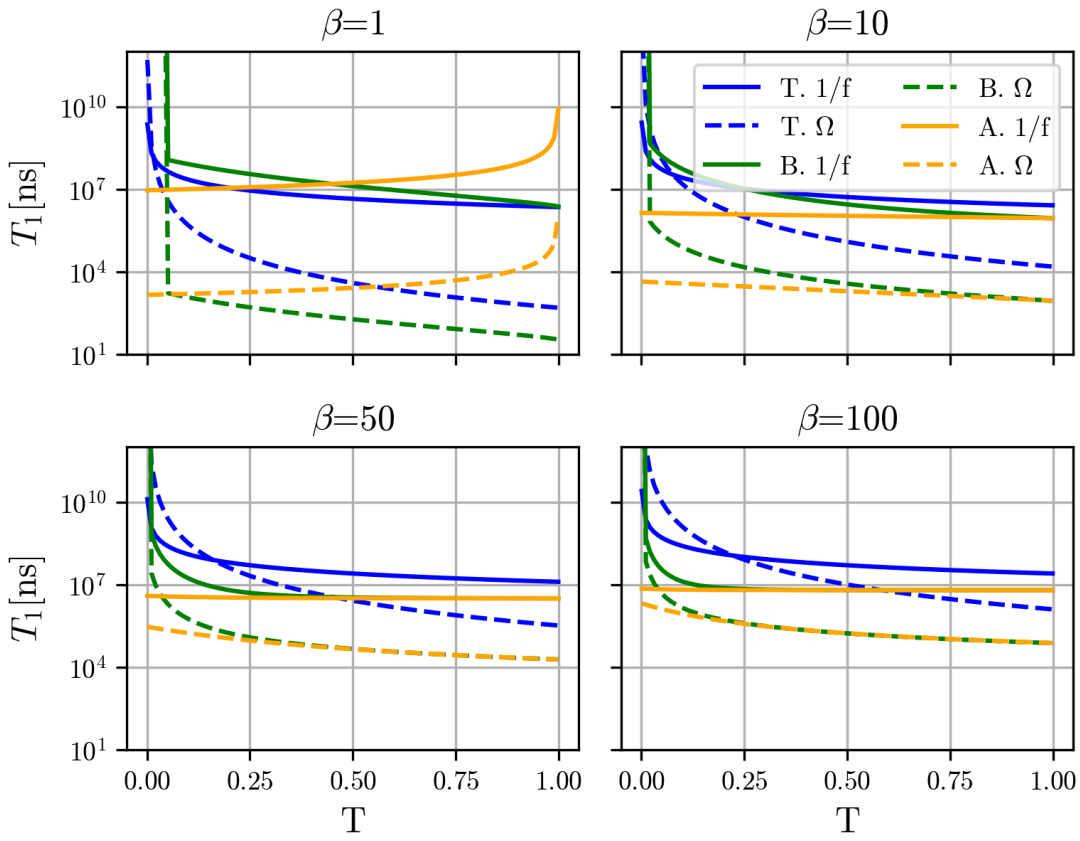

Figure 6.1: The T_1 times from both ohmic and $1/f$ noise is plotted at four different weights as a function of transmission T.

The diverging behaviour of Beenakker's Hamiltonian in the light, low transmission limit is because there is not two bound states in that case. In Beenakker's Hamiltonian the difference between the maximum and the minimum of the potential is $\approx T/2$. So in the low transmission limit we have a vary shallow potential. Combining this with the fact that when the system is light then the states do not lay deep in the potential. This means that as the transmission T is lowered then suddenly there is a point where the first excited state is not bound anymore and it quickly goes from a localised state to something that resembles a free particle.

This will drastically change the matrix element $|\langle 1|n|0\rangle|^2$ and the model breaks down.

At $\beta = 1$ in Figure 6.1 we see that the T_1 time for Averin's Hamiltonian actually increases as T goes to 1. We would expect it agree with Beenakker as we have specifically scaled to system so that is the case. What is going in here is that when β is high, then states lay deep in potential for Beenakker and in Averin lowest couple of state lay mostly in the same subspace. But as β decreases then the states from the other subspace get "pulled" down. So now when $T \to 1$ the two lowest states are almost in completely different subspaces. Those two states completely decouple at $T = 1$ so the matrix element goes to zero because,

$$\langle 1|A|0\rangle = (\Psi, \mathbb{0})(a \otimes I_2)\begin{pmatrix} \mathbb{0} \\ \Psi' \end{pmatrix} = 0, \tag{6.4.1}$$

where a is any linear operator. This vanishing of the matrix element is the reason that the T_1 time diverges for Averin's Hamiltonian.

Generally across all four plots in Figure 6.1 Averin has a lower T_1 time than Beenakker in the low transmission limit. This might be the explanation for the fact that the experimentalists get a lower than expected T_1 time, because they use Beenakker to model their gatemons. So it is tempting to say we have found the source of the discrepancy in the coherence times. But before we jump to that conclusion we have to make sure that this is the appropriate way of comparing the two models. What we have done here is all well and good from a purely theoretical perspective. But when the experimentalists build these devices they are not necessarily be able to tune the same parameters as we have been changing so far.

6.4.1 Experimentalist comparison

It turns out that in reality it is hard to know E_J. So when designing transmons the experimentalists parameterise the qubits by their capacitive energy E_C and the qubit frequency ω_q and then they calculate the Josephson energy E_J. They can do this because the transmons is heavy, so the wavefunction is localised around $\phi = 0$. We can then expand the $\cos(\phi)$ potential to 4^{th} order to get the Duffing oscillator[14]. Treating the 4^{th} order term as a perturbation Koch et al. finds an approximate equation for the qubit frequency,

$$\omega_q \approx \sqrt{8E_C E_J} - E_C \Rightarrow E_J \approx \frac{(\omega_q + E_C)^2}{8E_C}. \tag{6.4.2}$$

So to do the same kind of comparison we choose an E_C and since we know Δ we solve Averin's and Beenakker's Hamiltonians. Then using equation (6.4.2) and the qubit frequency from Beenakker's Hamiltonian we find what the appropriate E_J is so that we have a transmon with the same E_C and the same qubit frequency. The reason that we calculate E_J from Beenakker's Hamiltonian and not Averin's is that the experimentalists use Beenakker's Hamiltonian so that is what they would do. We then solve Beenakker's and Averin's Hamiltonian for a range of E_C from

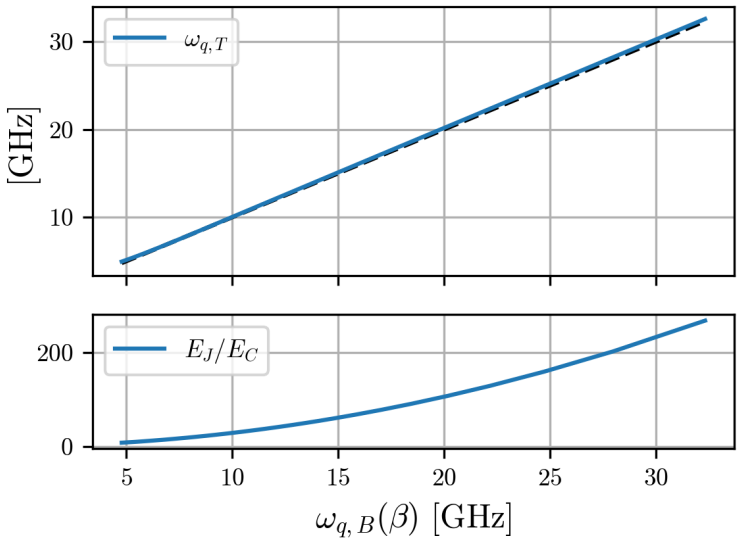

Figure 6.2: The frequency of the comparable transmon plotted against the frequency from Beenakker's Hamiltonian to test the validity of equation (6.4.2). The dashed line is $\omega_{q,B} = \omega_{q,T}$. The bottom plot is the weight of the comparable transmon.

$E_C = \Delta/5$ to $E_C = \Delta/60$. The first thing we do is then to test how well the approximation in Equation (6.4.2) works. As we can see in the top plot of Figure 6.2 the approximation works very well for $\omega_{q,B} > 5$GHz which is $\beta > 10$. So we have a gatemon and a transmon with the same E_C and approximately the same frequency. We can now make a proper comparison of the transmon and the two gatemons. Looking at figure 6.3 we can see that Averin's Hamiltonian has a worse T_1 time, but it seems most pronounced at low transmission. At low transmission it is a factor 2 to 3 which is pretty close to the factor 3-4 difference that the experimentalists find.

But when working with the gatemons E_C is not a parameter we can change after we have built the device. In Figure 6.4 we have plotted only the T_1 time from ohmic noise as we can see from Figure 6.3 that it is the limiting noise source. We can see that as long as we stay in the low transmission regime, then Averin's Hamiltonian gives significantly worse T_1 time.

We have not plotted the transmon her because the qubit frequency depends on the transmission. So for any T there is a corresponding transmon so it would not make sense to plot along side the two gatemon models in Figure 6.4. With this plot we can see that Averin's Hamiltonian has a wore T_1 time for a large range of frequencies. For $E_C = \Delta/50$ and $\Delta \approx 160$meV this range is exactly the operating range for gatemon qubits[17, 18, 43].

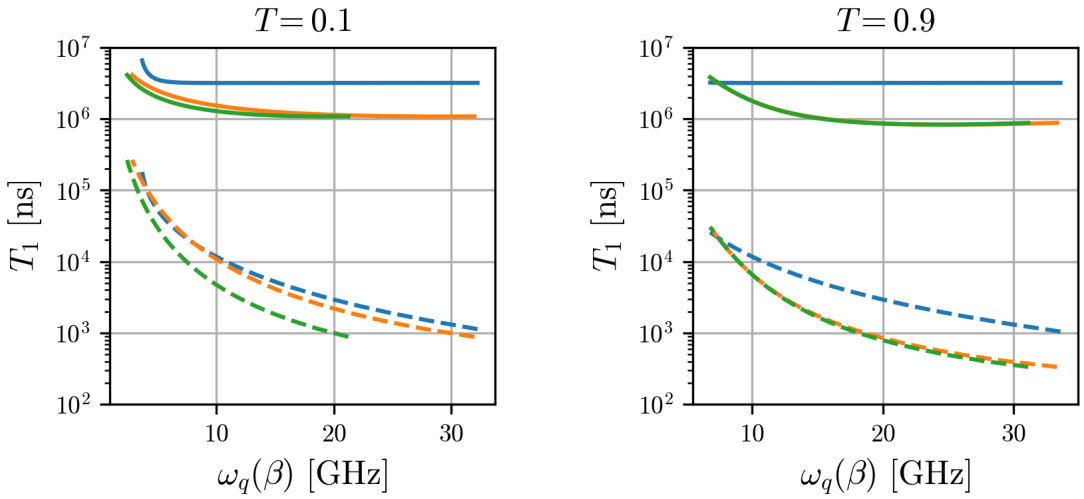

(a) (b)

Figure 6.3: The T_1 times for the three models with the same E_C and ω_q. The qubit frequency is varied by varying E_C from $\Delta/5$ to $\Delta/60$.

6.5 Circuits

Even though we have found a discrepancy in the T_1 times there might still be other effects that disproportionally affect the gatemon. When looking at possible sources of decoherence in qubits we cannot ignore the surrounding circuit's effect on the qubit. There is more to the environment than a general ohmic bath. Components like resonators or drive lines affect the qubit in very different ways. The first thing we do is restrict our selves to the two lowest energy states, so we can approximate the qubit as a harmonic oscillator. We do this because the harmonic oscillator is a system that we can solve exactly and we can use classical circuit theory with only resistors, indicators and capacitors to do this. The LC circuit that represents the qubit is put in parallel with an impedance that represents the environment. This is the method used by Houck et al.[44].

6.5.1 Circuit theory

To see where the equations Houck et al. uses come from, especially $R = 1/\mathrm{Re}\{Y\}$, it is illustrative to first look at the impedance of a regular LCR circuit. The reason that we will take a closer look at the derivation, is that $R = 1/\mathrm{Re}\{Y\}$ is generally only true when the complex part of the admittance, the susceptance, is zero. Normally $\mathrm{Re}\{Y\} = R/(R^2 + X^2)$ But in Houck et al. this relation is used even though the susceptance is not zero resulting in an effective resistance. The impedances of the individual components are,

$$Z_R = R \quad , \quad Z_C = \frac{1}{i\omega C} \quad , \quad Z_L = i\omega L. \tag{6.5.1}$$

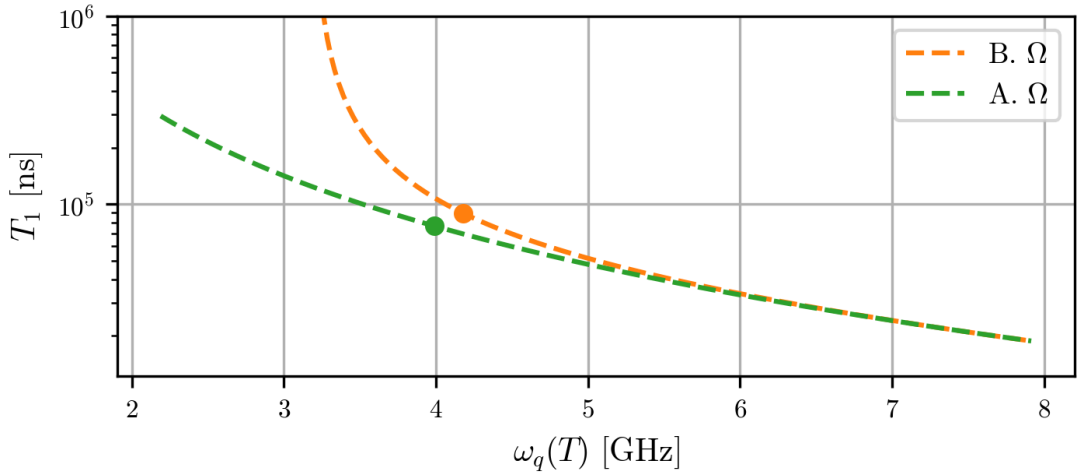

Figure 6.4: T_1 time from ohmic noise with $E_C = \Delta/50$. The dots indicate $T = 0.3$

We also use the relations for the Q-factor and resonance frequency, $Q = RC\omega_0$ and $\omega_0 = 1/\sqrt{LC}$[45]. The total impedance of a parallel LCR circuit is,

$$Z = \left(i\omega C_r + \frac{1}{i\omega L_r} + \frac{1}{R_r}\right)^{-1} = \frac{\omega}{iC_r}\left(\omega^2 - \omega_0^2 - \frac{i\omega\omega_0}{Q_r}\right)^{-1}, \tag{6.5.2}$$

and the relaxation time for the circuit is $T_1 = Q/\omega_0 = RC$ because then the last term becomes $i\omega/T_1$ and T_1 is the dampening time. The circuit diagram for a parallel LCR circuit can be seen in Figure 6.5 in the box labelled read-out resonator. But if we connect the LC circuit to a complex impedance instead of a real resistance then the equation looks a bit different,

$$\begin{aligned} Z &= \left(i\omega C_q + \frac{1}{i\omega L_q} + \frac{1}{Z_{env}(\omega)}\right)^{-1} \\ &= \left(i\omega C_q + \frac{1}{i\omega L_q} + Y_{env}(\omega)\right)^{-1} = \frac{\omega}{iC_q}\left(\omega^2 - \omega_0^2 - \frac{i\omega Y_{env}(\omega)}{C_q}\right)^{-1}, \end{aligned} \tag{6.5.3}$$

where C_q is the qubit capacitance. We split the admittance into its real and imaginary part $Y_{\text{env}} = \text{Re}\{Y_{\text{env}}\} + i\text{Im}\{Y_{\text{env}}\}$.

$$Z = \frac{\omega}{iC_q}\left(\omega^2 - \omega_0^2 + \frac{\omega\text{Im}\{Y_{\text{env}}(\omega)\}}{C_q} - \frac{i\omega\text{Re}\{Y_{\text{env}}(\omega)\}}{C_q}\right)^{-1}. \tag{6.5.4}$$

Comparing Equation (6.5.4) to (6.5.2) we see that the $\omega\text{Im}\{Y_{\text{env}}(\omega)\}/C_q$ term shifts the resonance frequency, whereas the $i\omega\text{Re}\{Y_{env}(\omega)\}/C_q$ term is imaginary so it corresponds to the $i\omega\omega_0/Q = i\omega/RC$ term in Equation (6.5.2). From this we can conclude that $\text{Re}\{Y_{\text{env}}(\omega)\}$ corresponds to the inverse of an effective resistance of the environment $\text{Re}\{Y_{\text{env}}(\omega)\} = 1/R_{\text{eff}}$. Using this, we calculate the T_1 time from the following equation $T_1 = C_q/\text{Re}\{Y_{\text{env}}(\omega)\}$. One of the simplest examples of this is if the qubit is capacitively coupled to a drive line with purely real

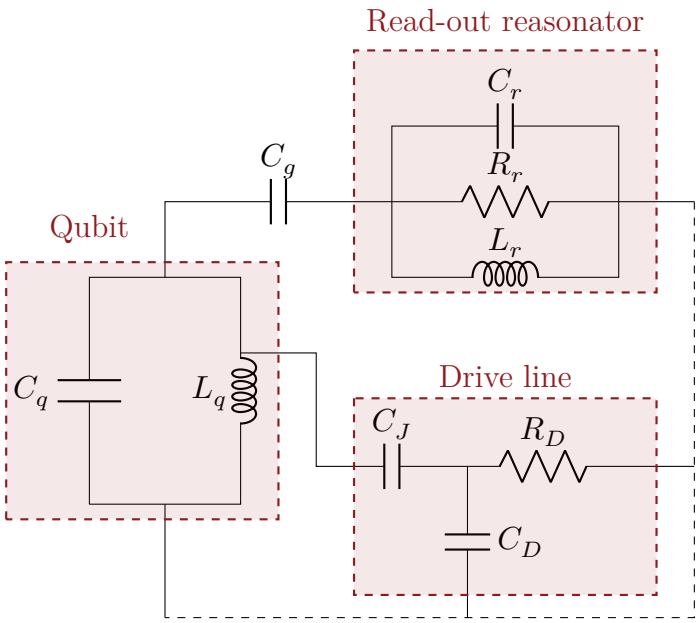

Figure 6.5: Circuit diagram of the qubit as a harmonic oscillator coupled to a read-out resonator and a drive line to voltage bias the nanowire. The black dashed line is ground.

impedance. This can be seen in Figure 6.5 as the components C_J and R_D. When calculating the admittance of the environment we include all components outside the qubit box in Figure 6.5. In this case the environment includes a capacitor with capacitance C_J and a resistor R_D in series. This drive line has admittance,

$$Y_{\mathrm{D}}(\omega) = \frac{1}{R + \frac{1}{i\omega C_J}} = \frac{i\omega C_J}{1 + i\omega C_J R} = \frac{\omega^2 C_J^2 R + i\omega C_J}{1 + \omega^2 C_J^2 R^2}. \tag{6.5.5}$$

$$\mathrm{Re}\left\{Y_{\mathrm{D}}(\omega)\right\} = \frac{\omega^2 C_J^2 R}{1 + \omega^2 C_J^2 R^2}. \tag{6.5.6}$$

The capacitance C_J is designed to be as small as possible. On current devices it is $C_J \approx 10^{-16}$F. Combined with $\omega \approx 10^9$Hz and $R = 50\Omega$ we can then drop the second term in the denominator as it is on the order of 10^{-10}. Then the T_1 time from coupling to the drive line is $T_{1,\mathrm{drive}} \approx C_q/\omega^2 C_J^2 R$. It decreases for high frequencies because capacitors generally let high frequencies through and block low frequencies. This can be seen in Equation (6.5.1) as the impedance of a capacitor decreases as the frequency increases. The consequence of this is that excitations have an easier time escaping out through the drive line if they have a high frequency leading to the lower T_1 time.

Another key component that the qubit couples to is the read-out resonator. The resonator is used to read out the qubit state. This is done by sweeping the frequencies and detecting the resonant frequency of the resonator. By modelling the resonator as a harmonic oscillator that couples to a two level system we get the James-Cummings Hamiltonian. In the James-Cummings Hamiltonian the resonant frequency of the resonator gets a slight shift depending on the state of the

two level system[46]. As we have already mentioned a resonator can be modelled as an LC circuit, but that is an ideal resonator which will never decay. A real resonator with a finite decay time and a finite Q-factor is modelled as an LCR-circuit. The qubit is again capacitively coupled to this component. The admittance of a capacitor in series with a parallel LCR circuit is,

$$Y_{\text{res}}(\omega) = \frac{1}{\frac{1}{i\omega C_g} + \frac{\omega}{iC_r}\left(\omega^2 - \omega_0^2 + \frac{i\omega\omega_0}{Q}\right)^{-1}}. \tag{6.5.7}$$

The real part of this expression can then be written as,

$$\text{Re}\left\{Y_{\text{res}}(\omega)\right\} = \frac{C_g^2\omega^4 R_r}{\left((C_r + C_g)\omega^2 - C_r\omega_0^2\right)^2 R_r^2 + \omega^2}, \tag{6.5.8}$$

where R_r is the resistance of the LCR ciruit. Assuming $C_g \ll C_r$ which is usually true as C_r is relatively large because it is the capacitance of the longe winding path in 6.6a. With that assumption we get,

$$\text{Re}\left\{Y_{\text{res}}(\omega)\right\} \approx \frac{C_g^2\omega^4 R_r}{\left(\omega^2 - \omega_0^2\right)^2 C_r^2 R_r^2 + \omega^2}. \tag{6.5.9}$$

When $\omega \gg \omega_0$ we can drop the ω_0^2 squared term and we get $C_g^2\omega^4 R/(\omega^4 C_r^2 R_r^2 + \omega^2)$. For large ω the ω^4 term will dominate the denominator and we end up with $\text{Re}\left\{Y_{\text{res}}(\omega)\right\} \approx (C_g/C_r)^2/R_r$ for $\omega \gg \omega_0$. So in the high frequency regime the real part of the admittance is frequency independent. The real part of the admittance has a maximum at ω_0 which is $\text{Re}\left\{Y_{\text{res}}(\omega_0)\right\} = C_g^2\omega_0^2 R_r$ and lastly $\text{Re}\left\{Y_{res}(0)\right\} = 0$. So once we take the inverse of Equation (6.5.9) the T_1 time from coupling to a resonator will have a minimum at the resonators resonance frequency which is to be expected. If the qubit was the same frequency as the resonator then the excitation in the qubit can easily escape and excite the resonator. A more interesting result from this is that if the ω_q is significantly higher than ω_0 then $T_1 \to C_q R(C_r/C_g)^2$, but if ω_q is significantly less than ω_0 then $T_1 \to \infty$. So driving the qubit at a frequency lower than the read-out resonators resonance frequency is generally better. There are some practical limitations like ω_q being high enough that fast operation are still possible, which means that we cannot go to extremely low values of ω_q.

6.5.2 Gatemon Circuit

To draw the circuit surrounding the gatemon we will look at the gatemon on the chip to see where there and how components couple to each other. Looking at Figure 6.6a we can see the read-out resonator capacitively coupled to the Cooper pair island. This is roughly the same for both transmons and gatemons, and is used to read out the qubit state. In Figure 6.6c we can see the drive line coming in from the top right and going under the nanowire. This is the big difference between the transmon and the gatemon. The drive line which controls the transmission

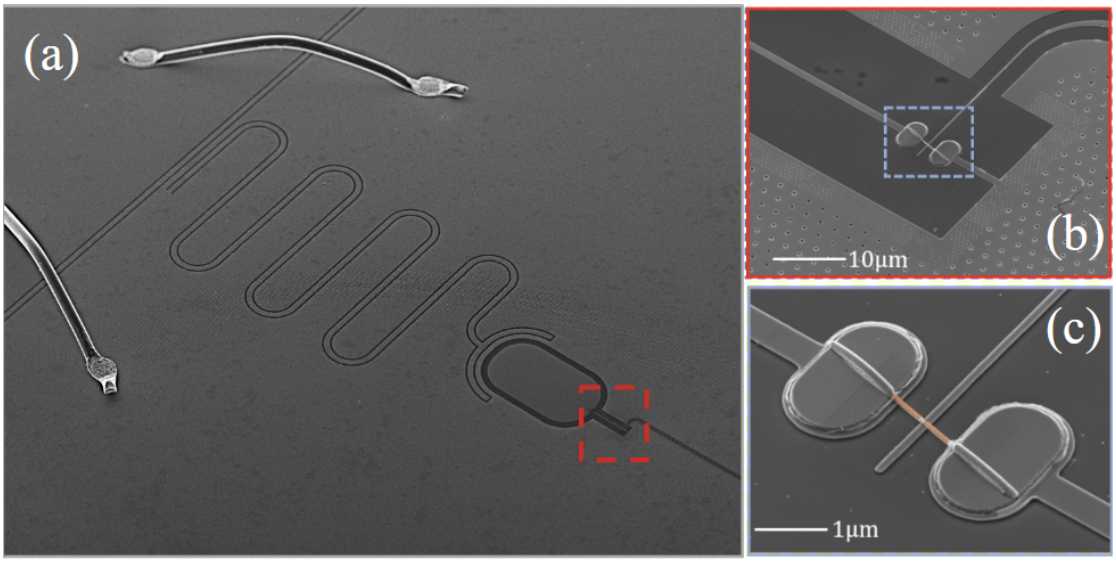

Figure 6.6: **(a)** The winding track is the read-out resonator and the oval shape is the Cooper pair island. **(b)** The line from the top right is the the drive line. **(c)** The orange line is the aluminium covered indium arsenide nanowire with the part over the drive line exposed. Credit to David Feldstein Bofill for the images.

will capacitively couple to the Cooper pair island which is the left oval. We will denote this capacitance C_J as it is near the junction. The drive line is impedance matched to $R_D = 50\Omega$. Zooming out to Figure 6.6b we can see how the drive line cuts through the ground plate in the top right. There will be a capacitance between the drive line and the ground plate C_D. Our theory is that the parasitic capacitance C_J will allow excitations to escape out to the drive line and either propagate down through the drive line or out to the ground plate through C_D. Incorporating this into the circuit analysis might yield the lower T_1 time that we have been looking for.

Drawing Figure 6.6 as a circuit diagram the qubit is represented as an LC circuit that is capacitively coupled to an LCR circuit which is the read-out resonator. The drive line is modelled as a capacitor and then a resistor and another capacitor in parallel. Including C_D in the circuit we calculate the admittance of the drive line with C_D and compare it to Equation (6.5.6).

$$Y_{\mathrm{D,cap}}(\omega) = \frac{1}{\frac{1}{i\omega C_J} + \frac{1}{i\omega C_D + \frac{1}{R}}} \quad , \quad \mathrm{Re}\left\{Y_{\mathrm{D,cap}}(\omega)\right\} = \frac{\omega^2 C_J^2 R}{1 + \omega^2 (C_D + C_J)^2 R^2}. \tag{6.5.10}$$

From this we see that if $C_D < 10^{-11}$F we recover Equation (6.5.6) and it has a negligible effect on the coherence time. One the other hand if $C_D > 10^{-11}$F then we can throw away C_J in the brackets as it is $\approx 10^{-16}$, but not C_D in the brackets. As we increase C_D the T_1 time actually improves. The reason that it increases the T_1 time is that we have inadvertently created a low-pass filter. Low-pass filters have a cut-off frequency which is given by $\omega_{\mathrm{cut}} = 1/RC$ and with $R = 50\Omega$ then a capacitance on the order of $\approx 10^{-11}$ will give a cut-off frequency

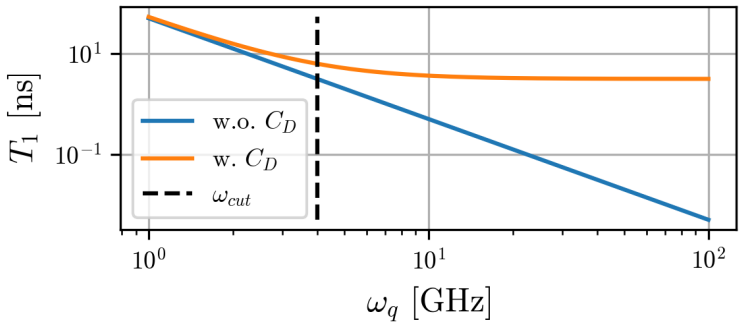

Figure 6.7: T_1 from the drive line with and with out C_D where $C_D = 5 \cdot 10^{-12}$ and $R_D = 50$.

of $\omega_{\text{cut}} \approx 2 \cdot 10^9$Hz and that is why we start seeing an effect at that frequency. When the cut-off frequency becomes lower than the qubit frequency the low-pass filter effectively blocks the excitation from escaping out through the drive line and that is why it leads to longer T_1 times. In figure 6.7 we can see T_1 from just the drive line with and with out C_D. C_D is chosen to be $5 \cdot 10^{-12}$ in this plot so the cutoff frequency is $\omega_{\text{cut}} = 4$GHz.

We then calculate the T_1 time for the entire environment. We have already done the heavy lifting of finding the real parts of the admittance for the resonator and the drive line separately. Admittances add in parallel, which from Figure 6.5, we can see the resonator and drive line are. So we simply add them to find the total admittance of everything outside the qubit box in Figure 6.5 and find T_1 through $T_1 = C_q/Y_{\text{total}}(\omega)$ with $Y_{\text{total}}(\omega) = Y_{\text{res}}(\omega) + Y_{\text{D}}(\omega)$. In Figure 6.8 we have plotted T_1 from the resonator alone and the resonator with the drive line with and without C_D. For the resonator alone we can see, as predicted that it is beneficial to drive the qubit at a lower frequency than the resonators resonance frequency. We can also see how including C_D in the calculations for the drive line improves the T_1 time when the qubit frequency ω_q is large.

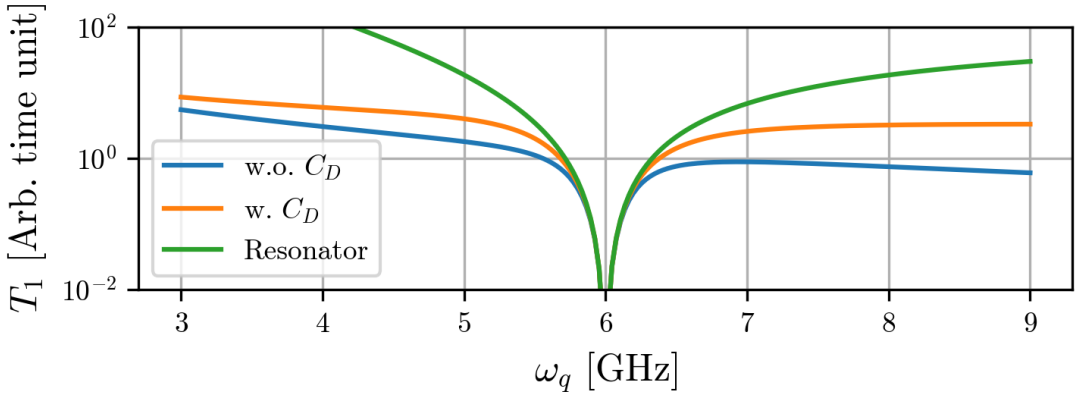

Figure 6.8: The T_1 calculated from the admittance of the resonator alone and with the drive line with and without the capacitance to ground C_D.

Chapter 7

Conclusion

In this thesis we have presented two different possible models for the gatemon qubit. We have attempted to derive an analytical expression for how they differ, but unfortunately this did not yield any useful results. We instead turned to numerical methods, solving the Hamiltonians with the finite difference method. Using the finite difference method we calculated the relaxation rates from ohmic and $1/f$ noise. With these results we see that when capacitive energy and operating frequency are held constant, then Averin's quantum point contact model results in lower T_1 times than Beenakker's model. The difference between the models is a factor 3 to 4 when the transmission is low. This is consistent with the difference between what the experimentalists measure and what current theory predicts.

The gatemon has different components around it on the chip. Specifically it has a drive line which is used to control the transmission of the nanowire. Even though the the result of the circuit analysis did not yield lower coherence times, we showed that increasing the capacitance between the drive line and the ground plate increases T_1 time. The gatemon does not seem to be limited by the drive line. This insight could be useful for future high frequency qubits which might be limited by coupling to drive lines, and then increasing the capacitance between the drive line and ground might just be thing that improves the T_1 time.

Further work is still needed to fully understand the behaviour of the gatemon. Another noise source we have not investigated in this thesis is dielectric loss. Dielectric loss is the loss from dissipation into the dielectric in the capacitor and around the qubit. The reason we did not investigate it in this thesis is it is highly material and manufacturing specific and beyond the scope of this thesis, but we have no reason to rule it out as a source of decoherence. As the T_1 times of the gatemons improve we will need to understand dephasing as well. So this will also need to be investigated for the gatemon to become a viable platform for a quantum computer.

Appendices

A Scattering matrix & Density of states

Looking at scattering as a time dependent perturbation as in Sakurai[47] we have the following expression for the scattering matrix

$$S_{ni} = \delta_{ni} - 2\pi i \delta(E_n - E_i) T_{ni}, \tag{A.1}$$

which is the matrix element for scattering from an initial state $|i\rangle$ to a final state $|n\rangle$. The T_{ni} is a matrix element of the T-matrix which is define so that it solves the equation,

$$\langle n|U_I(t,t_0)|i\rangle = \delta_{ni} - \frac{i}{\hbar} T_{ni} \int_{t_0}^{t} e^{i\omega_{ni}t' + \epsilon t'} dt'. \tag{A.2}$$

The T-matrix can be calculated by using the Lippman-Schwinger equation[47] and we get,

$$T = V + V \frac{1}{E_i - H_0 + i\varepsilon} T. \tag{A.3}$$

The fraction in the middle is the non-interacting retarded Green's function $G_0^R = 1/(E_i - H_0 + i\varepsilon)$. Inserting that we get the definition of the T matrix that Souma & Suzuki use[48], which is $T = V + VG_0^R T$. Using this result we can find that[49],

$$G^R(r,r';E) = G_0^R(r,r';E) + \iint dr_1 dr_2 G_0^R(r,r_1;E) T(r_1,r_2;E) G_0^R(r_2,r';E). \tag{A.4}$$

In the paper by Souma & Suzuki, from which this derivation is inspired by, they start by showing that the local density of states in real space is,

$$\rho(r,E) = \frac{-1}{\pi} \mathrm{Im}\left\{G^R(r,r;E)\right\}. \tag{A.5}$$

This result can also be found in textbooks such as "Electronic Transport in Mesoscopic Systems" by Supriyo Datta[50]. Inserting Equation (A.4) into (A.5) there are two parts. The first term simply gives a sum of delta function from free particles not interacting with the scattering potential. See for example equation (8.55) in Bruus and Flensberg[51]. We are interested in the second term, because that is the term that tells us how the local density of states chances from the introduction of the scattering potential. Since it is only the diagonal terms of the Green's

function (see Equation (A.5)) then we can hide away all the integrals and write it as,

$$\Delta\rho(r,E) = -\frac{1}{\pi}\mathrm{Im}\left\{\langle r|G_0^R(E)T(E)G_0^R(E)|r\rangle\right\}. \tag{A.6}$$

The change to the global density of states is then found from integrating Equation (A.6) over the entire volume. Since this is an integral over the diagonal terms it is the same as taking the trace.

$$\Delta\rho(E) = \int_V dr\Delta\rho(r,E) = -\frac{1}{\pi}\mathrm{Im}\left\{\mathrm{Tr}\{G_0^R(E)T(E)G_0^R(E)\}\right\}. \tag{A.7}$$

The rest of the derivation follows the appendix of Souma and Suzuki's paper[48]. Now we use the cyclic property of the trace to get $\mathrm{Tr}\{G_0^R(E)T(E)G_0^R(E)\} = \mathrm{Tr}\{G_0^R(E)G_0^R(E)T(E)\}$. Using the fact that the retarded Greens function can be written as $G^R(E) = [(E+i0^+)\hat{I} - \hat{H}]$ means that the following relation holds,

$$G^R(E)G^R(E) = -\frac{\partial G^R(E)}{\partial E}. \tag{A.8}$$

Inserting that we have,

$$\Delta D(E) = -\frac{1}{\pi}\mathrm{Im}\left\{\mathrm{Tr}\left\{-\frac{\partial G_0^R(E)}{\partial E}T(E)\right\}\right\}. \tag{A.9}$$

Another way of writing $T(E)$ is, $T(E) = V\sum_{n=0}^{\infty}(G^R(E)_0V)^n$ which then gives us,

$$\Delta\rho(E) = -\frac{1}{\pi}\mathrm{Im}\left\{\mathrm{Tr}\left\{-\frac{\partial G_0^R(E)}{\partial E}V\sum_{n=0}^{\infty}(G_0^R(E)V)^n\right\}\right\}. \tag{A.10}$$

collecting all the G_0^R's using,

$$\begin{aligned}\frac{\partial(VG_0^R(E))^n}{\partial E} &= n(VG_0^R(E))^{n-1}V\frac{\partial G_0^R(E)}{\partial E}\\ \Rightarrow (VG_0^R(E))^nV\frac{\partial G_0^R(E)}{\partial E} &= \frac{1}{n+1}\frac{\partial}{\partial E}\left(VG_0^R(E)\right)^{n+1}.\end{aligned} \tag{A.11}$$

Changing the limits of the sum it can be written as,

$$\Delta\rho(E) = -\frac{1}{\pi}\mathrm{Im}\left\{\mathrm{Tr}\left\{\frac{\partial}{\partial E}\sum_{n=1}^{\infty}\frac{-1}{n}(G_0^R(E)V)^n\right\}\right\}. \tag{A.12}$$

This sum has a closed form solution which is,

$$\Delta\rho(E) = -\frac{1}{\pi}\mathrm{Im}\left\{\frac{\partial}{\partial E}\mathrm{Tr}\left\{\ln\left(\hat{I} - G_0^RV\right)\right\}\right\} \tag{A.13}$$

Taking the imaginary part of a complex number can be expressed as $\mathrm{Im}\{z\} = (z-z^*)/(2i)$.

$$\Delta\rho(E) = -\frac{1}{2\pi i}\frac{\partial}{\partial E}\mathrm{Tr}\left\{\ln\left(\hat{I} - G_0^RV\right) - \ln\left(\hat{I} - G_0^AV\right)\right\} \tag{A.14}$$

$$= \frac{\partial}{\partial E}\frac{1}{2\pi i}\mathrm{Tr}\left\{\ln\left(\frac{\hat{I} - G_0^AV}{\hat{I} - G_0^RV}\right)\right\}, \tag{A.15}$$

where we've used that $[G_0^R]^* = G_0^A$[51]. For the next step we'll need that $T = V + G_0^R T \Rightarrow T = V/(1 - G_0^R V)$. The term with in the logarithm can then be written as,

$$\frac{\hat{I} - G_0^A V}{\hat{I} - G_0^R V} = \frac{\hat{I}}{\hat{I} - G_0^R V} - G_0^A \frac{V}{\hat{I} - G_0^R V} \tag{A.16}$$

$$= \frac{I - G_0^R \hat{V} + G_0^R V}{\hat{I} - G_0^R V} - G_0^A T \tag{A.17}$$

$$= 1 + G_0^R T - G_0^A T. \tag{A.18}$$

So the change in the density of states is,

$$\Delta\rho(E) = \frac{1}{2\pi i} \frac{\partial}{\partial E} \mathrm{Tr}\Big\{\ln\Big(\hat{I} - (G_0^A - G_0^R)T\Big)\Big\}. \tag{A.19}$$

Once again we will use $[G_0^R]^* = G_0^A$ and $\mathrm{Im}\{z\} = (z - z^*)/(2i)$. We then see that we can rewrite the Green's functions,

$$G_0^A - G_0^R = [G_0^R]^* - G_0^R = -i2\mathrm{Im}\left\{G_0^R\right\} = iA_0(E) = 2\pi i\delta(E - H_0). \tag{A.20}$$

Inserting that,

$$\Delta\rho(E) = \frac{1}{2\pi i} \frac{\partial}{\partial E} \mathrm{Tr}\Big\{\ln\Big(\hat{I} - 2\pi i\delta(E - H_0)T\Big)\Big\}. \tag{A.21}$$

But the term in the logarithm is exactly our scattering matrix from the beginning (A.1) so we get,

$$\Delta\rho(E) = \frac{1}{2\pi i} \frac{\partial}{\partial E} \mathrm{Tr}\{\ln(S(E))\}. \tag{A.22}$$

Bibliography

1. Feynman, R. P. Simulating Physics with Computers. *International Journal of Theoretical Physics* **21,** 467–488. ISSN: 0020-7748, 1572-9575. http://link.springer.com/10.1007/BF02650179 (2024) (June 1982).
2. Robert, A., Barkoutsos, P. K., Woerner, S. & Tavernelli, I. Resource-Efficient Quantum Algorithm for Protein Folding. *npj Quantum Information* **7,** 38. ISSN: 2056-6387. https://www.nature.com/articles/s41534-021-00368-4 (2024) (Feb. 17, 2021).
3. Rubin, N. C. *et al. Quantum Computation of Stopping Power for Inertial Fusion Target Design* arXiv: 2308.12352 [physics, physics:quant-ph]. http://arxiv.org/abs/2308.12352 (2023). preprint.
4. Shor, P. W. Polynomial-Time Algorithms for Prime Factorization and Discrete Logarithms on a Quantum Computer. *SIAM Journal on Computing* **26,** 1484–1509. ISSN: 0097-5397, 1095-7111. http://epubs.siam.org/doi/10.1137/S0097539795293172 (2024) (Oct. 1997).
5. Mavroeidis, V., Vishi, K., Zych, M. D. & Jøsang, A. The Impact of Quantum Computing on Present Cryptography. *International Journal of Advanced Computer Science and Applications* **9.** ISSN: 21565570, 2158107X. arXiv: 1804.00200 [cs]. http://arxiv.org/abs/1804.00200 (2024) (2018).
6. Resch, S. & Karpuzcu, U. R. *Quantum Computing: An Overview Across the System Stack* arXiv: 1905.07240 [quant-ph]. http://arxiv.org/abs/1905.07240 (2024). preprint.
7. Dail, O. *Eagle's Quantum Performance Progress | IBM Quantum Computing Blog* IBM. https://ibm.com/quantum/blog/eagle-quantum-processor-performance (2024).
8. Blais, A., Huang, R.-S., Wallraff, A., Girvin, S. M. & Schoelkopf, R. J. Cavity Quantum Electrodynamics for Superconducting Electrical Circuits: An Architecture for Quantum Computation. *Physical Review A* **69,** 062320. https://link.aps.org/doi/10.1103/PhysRevA.69.062320 (2023) (June 29, 2004).
9. Mabuchi, H. & Doherty, A. C. Cavity Quantum Electrodynamics: Coherence in Context. *Science* **298,** 1372–1377. ISSN: 0036-8075, 1095-9203. https://www.science.org/doi/10.1126/science.1078446 (2024) (Nov. 15, 2002).

10. Rasmussen, S. E. *et al.* The Superconducting Circuit Companion – an Introduction with Worked Examples. *PRX Quantum* **2,** 040204. ISSN: 2691-3399. arXiv: 2103.01225 [cond-mat, physics:quant-ph]. http://arxiv.org/abs/2103.01225 (2023) (Dec. 14, 2021).

11. Annett, J. F. *Superconductivity, Superfluids, and Condensates* 186 pp. ISBN: 978-0-19-850755-0 978-0-19-850756-7 (Oxford University Press, Oxford ; New York, 2004).

12. Vool, U. & Devoret, M. H. Introduction to Quantum Electromagnetic Circuits. *International Journal of Circuit Theory and Applications* **45,** 897–934. ISSN: 0098-9886, 1097-007X. arXiv: 1610.03438 [cond-mat, physics:quant-ph]. http://arxiv.org/abs/1610.03438 (2023) (July 2017).

13. Aumann, P., Menke, T., Oliver, W. D. & Lechner, W. CircuitQ: An Open-Source Toolbox for Superconducting Circuits. *New Journal of Physics* **24,** 093012. ISSN: 1367-2630. arXiv: 2106.05342 [quant-ph]. http://arxiv.org/abs/2106.05342 (2023) (Sept. 1, 2022).

14. Koch, J. *et al.* Charge-Insensitive Qubit Design Derived from the Cooper Pair Box. *Physical Review A* **76,** 042319. ISSN: 1050-29470556-2791. https://ui.adsabs.harvard.edu/abs/2007PhRvA..76d2319K (2023) (Oct. 1, 2007).

15. Acharya, R. *et al.* Suppressing Quantum Errors by Scaling a Surface Code Logical Qubit. *Nature* **614,** 676–681. ISSN: 1476-4687. https://www.nature.com/articles/s41586-022-05434-1 (2024) (Feb. 2023).

16. Danilenko, A. *et al.* Few-Mode to Mesoscopic Junctions in Gatemon Qubits. *Physical Review B* **108,** L020505. https://link.aps.org/doi/10.1103/PhysRevB.108.L020505 (2023) (July 17, 2023).

17. Kringhøj, A. *et al.* Anharmonicity of a Gatemon Qubit with a Few-Mode Josephson Junction. *Physical Review B* **97,** 060508. ISSN: 2469-9950, 2469-9969. arXiv: 1703.05643 [cond-mat]. http://arxiv.org/abs/1703.05643 (2023) (Feb. 21, 2018).

18. Casparis, L. *et al.* Gatemon Benchmarking and Two-Qubit Operations. *Physical Review Letters* **116,** 150505. https://link.aps.org/doi/10.1103/PhysRevLett.116.150505 (2023) (Apr. 15, 2016).

19. Beenakker, C. W. J. Universal Limit of Critical-Current Fluctuations in Mesoscopic Josephson Junctions. *Physical Review Letters* **67,** 3836–3839. ISSN: 0031-9007. https://link.aps.org/doi/10.1103/PhysRevLett.67.3836 (2023) (Dec. 30, 1991).

20. Averin, D. V. Coulomb Blockade in Superconducting Quantum Point Contacts. *Physical Review Letters* **82,** 3685–3688. ISSN: 0031-9007, 1079-7114. https://link.aps.org/doi/10.1103/PhysRevLett.82.3685 (2023) (May 3, 1999).

21. Sauls, J. A. Andreev Bound States and Their Signatures. *Philosophical Transactions of the Royal Society A: Mathematical, Physical and Engineering Sciences* **376,** 20180140. ISSN: 1364-503X, 1471-2962. arXiv: 1805.11069 [cond-mat]. http://arxiv.org/abs/1805.11069 (2023) (Aug. 6, 2018).

22. Abadir, K. M. & Magnus, J. R. *Matrix Algebra* ISBN: 978-0-511-64796-3 (Cambridge University Press, Cambridge, 2005).

23. Van Wees, B. J. *et al.* Quantized Conductance of Point Contacts in a Two-Dimensional Electron Gas. *Physical Review Letters* **60,** 848–850. ISSN: 0031-9007. https://link.aps.org/doi/10.1103/PhysRevLett.60.848 (2024) (Feb. 29, 1988).

24. Lauwens, J., Kerkhofs, L., Sala, A. & Sorée, B. *Superconductor-Semiconductor Hybrid Capacitance with a Nonlinear Charge-Voltage Profile* arXiv: 2306.09091 [cond-mat]. http://arxiv.org/abs/2306.09091 (2024). preprint.

25. Hart, S. *et al.* Current-Phase Relations of InAs Nanowire Josephson Junctions: From Interacting to Multimode Regimes. *Physical Review B* **100,** 064523. ISSN: 2469-9950, 2469-9969. https://link.aps.org/doi/10.1103/PhysRevB.100.064523 (2024) (Aug. 26, 2019).

26. Schoelkopf, R. J., Clerk, A. A., Girvin, S. M., Lehnert, K. W. & Devoret, M. H. *Qubits as Spectrometers of Quantum Noise* arXiv: cond-mat/0210247. http://arxiv.org/abs/cond-mat/0210247 (2024). preprint.

27. Fetter, A. L. & Walecka, J. D. *Theoretical Mechanics of Particles and Continua* 570 pp. ISBN: 978-0-486-43261-8 (Dover Publications, Mineola, N.Y, 2003).

28. Johnson, J. B. Thermal Agitation of Electricity in Conductors. *Physical Review* **32,** 97–109. ISSN: 0031-899X. https://link.aps.org/doi/10.1103/PhysRev.32.97 (2024) (July 1, 1928).

29. Nyquist, H. Thermal Agitation of Electric Charge in Conductors. *Physical Review* **32,** 110–113. ISSN: 0031-899X. https://link.aps.org/doi/10.1103/PhysRev.32.110 (2024) (July 1, 1928).

30. Caldeira, A. & Leggett, A. Quantum Tunnelling in a Dissipative System. *Annals of Physics* **149,** 374–456. ISSN: 00034916. https://linkinghub.elsevier.com/retrieve/pii/0003491683902026 (2024) (Sept. 1983).

31. *Noise in Physical Systems and 1/f Fluctuations: St. Louis, MO 1993* (eds Handel, P. H. & Chung, A. L.) *AIP Conference Proceedings* **285.** 757 pp. ISBN: 978-1-56396-270-7 (American Institute of Physics, New York, NY, 1993).

32. Bonanno, G., Lillo, F. & Mantegna, R. N. Dynamics of the Number of Trades of Financial Securities. *Physica A: Statistical Mechanics and its Applications* **280,** 136–141. ISSN: 03784371. arXiv: cond-mat/9912006. http://arxiv.org/abs/cond-mat/9912006 (2024) (May 2000).

33. Flinn, I. Extent of the 1/f Noise Spectrum. *Nature* **219,** 1356–1357. ISSN: 1476-4687. https://www.nature.com/articles/2191356a0 (2024) (5161 Sept. 1968).

34. Van Der Ziel, A. in *Advances in Electronics and Electron Physics* 225–297 (Elsevier, 1979). ISBN: 978-0-12-014649-9. https://linkinghub.elsevier.com/retrieve/pii/S0065253908607684 (2024).

35. Bernamont, J. Fluctuations de Potentiel Aux Bornes d'un Conducteur Métallique de Faible Volume Parcouru Par Un Courant. *Annales de physique* **11,** 71–140. ISSN: 0003-4169, 1286-4838. http://www.annphys.org/10.1051/anphys/193711070071 (2024) (1937).

36. Milotti, E. 1/f Noise: A Pedagogical Review. *Arxiv: Physics* (May 12, 2002).

37. Miller, S. L. & Childers, D. G. *Probability and Random Processes: With Applications to Signal Processing and Communications* 2nd. ed. ISBN: 978-0-12-386981-4 (Academic Press, Boston, MA, 2012).

38. Krøjer, S., Dahl, A. E., Christensen, K. S., Kjaergaard, M. & Flensberg, K. *Fast Universal Control of a Flux Qubit via Exponentially Tunable Wave-Function Overlap* arXiv: 2303.01102 [cond-mat, physics:quant-ph]. http://arxiv.org/abs/2303.01102 (2023). preprint.

39. Groszkowski, P. *et al.* Coherence Properties of the 0- Qubit. *New Journal of Physics* **20,** 043053. ISSN: 1367-2630. https://dx.doi.org/10.1088/1367-2630/aab7cd (2023) (Apr. 2018).

40. Zorin, A. B. *et al.* Background Charge Noise in Metallic Single-Electron Tunneling Devices. *Physical Review B* **53,** 13682–13687. https://link.aps.org/doi/10.1103/PhysRevB.53.13682 (2024) (May 15, 1996).

41. Yan, F. *et al.* The Flux Qubit Revisited to Enhance Coherence and Reproducibility. *Nature Communications* **7,** 12964. ISSN: 2041-1723. https://www.nature.com/articles/ncomms12964 (2024) (Nov. 3, 2016).

42. Court, N. A., Ferguson, A. J. & Clark, R. G. Energy Gap Measurement of Nanostructured Aluminium Thin Films for Single Cooper-pair Devices. *Superconductor Science and Technology* **21,** 015013. ISSN: 0953-2048, 1361-6668. https://iopscience.iop.org/article/10.1088/0953-2048/21/01/015013 (2024) (Jan. 1, 2008).

43. Larsen, T. W. *et al.* Semiconductor-Nanowire-Based Superconducting Qubit. *Physical Review Letters* **115,** 127001. https://link.aps.org/doi/10.1103/PhysRevLett.115.127001 (2023) (Sept. 14, 2015).

44. Houck, A. A. *et al.* Controlling the Spontaneous Emission of a Superconducting Transmon Qubit. *Physical Review Letters* **101,** 080502. ISSN: 0031-9007, 1079-7114. https://link.aps.org/doi/10.1103/PhysRevLett.101.080502 (2024) (Aug. 21, 2008).

45. *Lecture Notes | Introduction to Electronics, Signals, and Measurement | Electrical Engineering and Computer Science* MIT OpenCourseWare. https://ocw.mit.edu/courses/6-071j-introduction-to-electronics-signals-and-measurement-spring-2006/pages/lecture-notes/ (2024).

46. Krantz, P. *et al.* A Quantum Engineer's Guide to Superconducting Qubits. *Applied Physics Reviews* **6,** 021318. ISSN: 1931-9401. arXiv: 1904.06560 [cond-mat, physics:physics, physics:quant-ph]. http://arxiv.org/abs/1904.06560 (2023) (June 1, 2019).

47. Sakurai, J. J. & Napolitano, J. *Modern Quantum Mechanics* 3rd ed. ISBN: 978-1-108-47322-4 (Cambridge University Press, Cambridge, 2021).

48. Souma, S. & Suzuki, A. Local Density of States and Scattering Matrix in Quasi-One-Dimensional Systems. *Physical Review B* **65,** 115307. ISSN: 0163-1829, 1095-3795. https://link.aps.org/doi/10.1103/PhysRevB.65.115307 (2024) (Feb. 19, 2002).

49. Economou, E. N. *Green's Functions in Quantum Physics* (red. Cardona, M. *et al.*) ISBN: 978-3-540-28838-1 978-3-540-28841-1. http://link.springer.com/10.1007/3-540-28841-4 (2024) (Springer Berlin Heidelberg, Berlin, Heidelberg, 2006).

50. Datta, S. *Electronic Transport in Mesoscopic Systems* 1. paperback pr., 8. print. *Cambridge Studies in Semiconductor Physics and Microelectronic Engineering* **3.** 377 pp. ISBN: 978-0-521-59943-6 (Cambridge Univ. Press, Cambridge, 2009).

51. Bruus, H. & Flensberg, K. *Many-Body Quantum Theory in Condensed Matter Physics: An Introduction* 435 pp. ISBN: 978-0-19-856633-5 (Oxford University Press, Oxford ; New York, 2004).